Insights into the dynamics of ligand-induced dimerisation via mathematical modelling and analysis

White, C.; Rottschäfer, V.; Bridge, L.J.

Journal of Theoretical Biology 538 (2022) 110996

Contents lists available at ScienceDirect

Journal of Theoretical Biology

journal homepage: www.elsevier.com/locate/yjtbi

Insights into the dynamics of ligand-induced dimerisation via mathematical modelling and analysis

C. White [a], V. Rottschäfer [b,c,*], L.J. Bridge [d]

[a] Swansea University, Swansea, UK
[b] Leiden University, Leiden, The Netherlands
[c] University of Amsterdam, Amsterdam, The Netherlands
[d] University of the West of England, Bristol, UK

ARTICLE INFO

Article history:
Received 16 September 2021
Revised 8 December 2021
Accepted 20 December 2021
Available online 24 January 2022

Keywords:
Mathematical pharmacology
Receptor theory
Differential equations
Perturbation methods
Dimerisation

ABSTRACT

The vascular endothelial growth factor (VEGF) receptor (VEGFR) system plays a role in cancer and many other diseases. It is widely accepted that VEGFR receptors dimerise in response to VEGF binding. However, analysis of these mechanisms and their implications for drug development still requires further exploration. In this paper, we present a mathematical model representing the binding of VEGF to VEGFR and the subsequent ligand-induced dimerisation. A key factor in this work is the qualitative and quantitative effect of binding cooperativity, which describes the effect that the binding of a ligand to a receptor has on the binding of that ligand to a second receptor, and the dimerisation of these receptors. We analyse the ordinary differential equation system at equilibrium, giving analytical solutions for the total amount of ligand bound. For time-course dynamics, we use numerical methods to explore possible behaviours under various parameter regimes, while perturbation analysis is used to understand the intricacies of these behaviours. Our simulation results show an excellent fit to experimental data, towards validating the model.

1. Introduction

Classical pharmacological receptor theory was originally based around assumptions of monomeric receptors detecting ligands (Kenakin, 2009). In recent years, the possibility for dimerised or higher-oligomerised receptors has been acknowledged (Milligan, 2004; Milligan, 2006; Milligan et al., 2013). New theoretical insights into binding and functional consequences of G protein-coupled receptors which exist as dimers have been provided by mathematical models (White and Bridge, 2019; Franco et al., 2005; Franco et al., 2006; Zhou and Giraldo, 2018). These models concern the dynamics and equilibria of binding and signalling outcomes of ligands at constitutively formed (pre-existing) dimers. The linear differential equation ligand-binding models in White and Bridge (2019) are specific to the pre-dimerised scenarios explored for adenosine receptors in May et al. (2011). Subtle, yet important, adjustment to these models is necessary to model the receptor dimerisation process which is triggered by ligand binding for other receptors.

Vascular endothelial growth factor (VEGF) is a signalling protein that is a key mediator of angiogenesis, a process whereby new blood vessels are formed from the pre-existing vasculature (Mac Gabhann and Popel, 2007; Alarcón and Page, 2007). As angiogenesis is a key factor in many conditions, including cancer and inflammation (Mac Gabhann and Popel, 2007; Shibuya, 2011; Peach et al., 2018), research into the mechanism of VEGF binding and signalling is essential towards progress in development of new therapies. The VEGF family consists of five members, VEGF-A, -B, -C, -D and placenta growth factor (PlGF), and is a sub-family of growth factors (GFs). Similar to most GFs, VEGF is a multivalent ligand, in that each molecule possesses more than one binding site, therefore, it can bind with as many receptors as there are sites (Alarcón and Page, 2007). Many aspects of cellular function, including survival, proliferation, migration and differentiation are regulated by VEGF (Gopalakrishnan et al., 2004; Olsson et al., 2006; Stuttfeld and Ballmer-Hofer, 2009).

VEGF binds to three VEGF receptors (VEGFRs), namely VEGFR-1, −2 and −3. These are receptor tyrosine kinases that are expressed predominately on endothelial cells and regulated by the VEGF ligand (Olsson et al., 2006). Like most other receptor tyrosine kinases (RTK), activation occurs upon dimerisation (Mac Gabhann and Popel, 2007; Alarcón and Page, 2007; Stuttfeld and Ballmer-

* Corresponding author at: Leiden University, Leiden, The Netherlands.
E-mail address: vivi@math.leidenuniv.nl (V. Rottschäfer).

https://doi.org/10.1016/j.jtbi.2021.110996
0022-5193/

Hofer, 2009). It is thought that VEGFRs diffuse across the cell membrane as monomeric receptors, although there is recent evidence suggesting that a percentage may exist as dimers (Maruyama, 2014) (also see references within). Binding of a ligand to the extracellular domain of the receptor triggers dimerisation with adjacent receptors, which leads to the receptors becoming activated, then leading to trans-autophosphorylation of the receptors. This provides a docking site for downstream signalling proteins, which results in the activation of signalling pathways, and ultimately a response (Olsson et al., 2006; Maruyama, 2014; Mac Gabhann and Popel, 2007).

Although advances have been made towards understanding the interactions of RTK ligands and receptors, further research is needed to fully understand their role as therapeutic targets (Peach et al., 2018; Peach et al., 2019; Shibuya, 2011). While much analysis assumes equilibrium (Mac Gabhann and Popel, 2007), a recent study (Kilpatrick et al., 2017) has used new technologies to provide a real time quantitative evaluation of VEGF-VEGFR binding. Developments in fluorescent ligand technologies have allowed the complexities of ligand-receptor interactions in living cells to be observed (Kilpatrick et al., 2017; Peach et al., 2018). Interaction dynamics were explored by monitoring the binding of dual poled VEGF ligand molecules (ligands which can bind two receptors simultaneously) to VEGFR-2 receptors. For quantification purposes, ligand binding timecourse results were fitted to a simple association exponential model; however, in many cases the results failed to fit with the standard model for simple mass-action equilibrium. Hence there is need for a mathematical model that incorporates the complexities of the VEGF binding dynamics, taking into account the ligand-induced dimerisation (LID).

The LID process is modelled in Alarcón and Page (2007), where multiple stochastic models are analysed to further understand the role the VEGF receptor system plays in tumour growth, although most models given there include biological processes beyond binding. Spatial models of the dimerisation process and subsequent signalling are developed in Mayawala et al. (2006), while dynamics of receptor and transducer protein dimerisation are studied using an ordinary differential equation (ODE) model in Vera et al. (2008), wherein it is suggested that dimerisation may serve to regulate signalling over multiple time scales. An ODE model of receptor binding and aggregation is presented in Wanant and Quon (2000), although only equilibrium is analysed. Equilibrium models in Wofsy et al. (1992) and Klein et al., 2004 also explore the possibility of heterodimers. Mac Gabhann and Popel (2007) combine a LID model with a *dynamic pre-dimerisation* model, whereby the dimers are formed before ligand binding, in order to explore the mechanisms of the dimerisation of VEGFR and the possibility of the VEGF receptors having the ability to dimerise in the absence of ligand as well as being induced by ligand. While a partial differential equation model for the evolution of all species is formulated, the dynamics of LID were not simulated or explored in detail.

Key to the formulation of our previous GPCR dimer models (White and Bridge, 2019) was the idea of binding *cooperativity*. Mathematically, this manifests as a parameter which quantifies the altered binding rate of a second ligand molecule to a preformed dimer, due to a first ligand already being bound. Analytical expressions for both equilibrium concentration curves and binding kinetics, in terms of cooperativity factors gave insights into the effects of crosstalk across the dimer on binding. Binding cooperativity is also an important concept in a model of LID, whereby the cooperativity factor now quantifies the altered binding rate of a second receptor molecule to a dual-poled ligand, due to a first receptor already being bound.

In this paper, we present and analyse a model for the dynamics of ligand-binding and LID. Our aim is to contribute to receptor theory by analysing the ligand-receptor interaction in detail without considering downstream signalling. We formulate a LID model similar to Mac Gabhann and Popel (2007), focussing on dimerisation and binding only, with explicit dependence on cooperativity factors (so following the framework of White and Bridge (2019)). The analytical solution methods for the linear ODE models in White and Bridge (2019) are not available to us here, as the LID model is nonlinear. We find numerical solutions for a range of control parameters, to explore possible time course behaviours. Further, we use perturbation analysis inline with nonlinear GPCR activation models (Woodroffe et al., 2009; Woodroffe et al., 2010; Bridge et al., 2010) to give further insights through analytical solutions for reduced problems under interesting parameter regimes.

The remainder of this paper is organised as follows. In Section 2, we formulate a nonlinear ODE model for LID dynamics. In Section 3, we follow the receptor theory approach of deriving equilibrium solutions, and in particular consider the effect of the *equilibrium cooperativity factor* on log-concentration response curves. In Section 4, we present typical timecourse results given by numerical simulations, considering the effects of *kinetic cooperativity factors*. To gain further insights into the dynamics, we nondimensionalise the ODE system, then find asymptotic solutions under parameter regimes of interest (Section 5). In Section 6, we fit our model to recently published timecourse data for VEGF-A isoforms binding at the VEGFR2 receptor, showing excellent agreement and plausible parameter values. We conclude in Section 7 with a discussion of our main results and contribution to the literature.

2. Model formulation

In formulating the model we assume that all receptors exist constitutively as monomers, represented by R, while ligand A is a

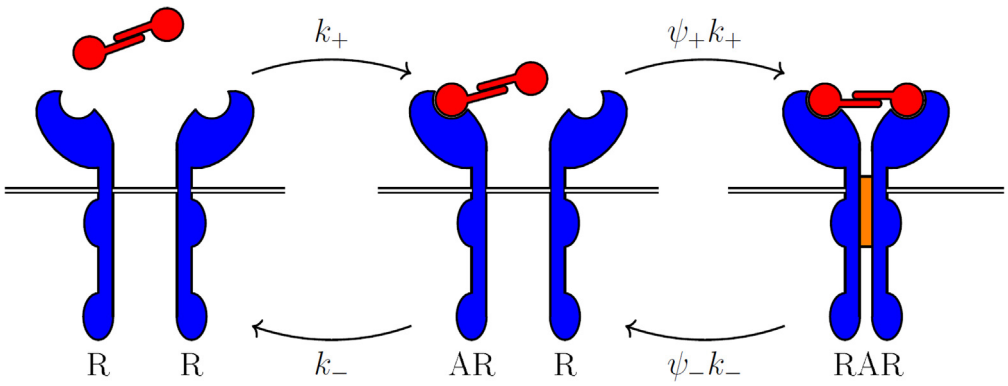

Fig. 2.1. Ligand binding and dimerisation is a two step process whereby a two poled ligand (in red) first binds a monomeric receptor (blue) before then binding a second and instantaneously dimerising the monomers.

two-poled ligand, which may be bound to two receptors simultaneously. Ligand binding and dimerisation is a two step process which can be visualised as in Fig. 2.1 or given as a reaction scheme in Fig. 2.2. In the first reversible reaction the ligand, whose concentration is assumed constant, binds to a free monomeric receptor, with association and dissociation rate constants k_+ and k_- respectively, creating the complex *AR*. Once a ligand molecule is bound to a receptor the ligand may reversibly bind a second receptor monomer, simultaneously dimerising the two receptors. We define the parameter $\psi = \psi_+/\psi_-$ as the equilibrium cooperativity factor, describing the ligand's increased (or decreased) affinity for the second receptor binding due to the first ligand pole being bound. If, for example, $\psi_+ > 1$ we have positive forward cooperativity, where the rate of a second receptor binding is greater than the binding rate of the first receptor, and negative forward cooperativity if $\psi_+ < 1$. We emphasise the difference in meaning of binding cooperativity between the current model and the pre-dimerised GPCR model of White and Bridge (2019); in White and Bridge (2019), the cooperativity considered gives a change in affinity of a second ligand binding, whereas here cooperativity describes the change in affinity of a second receptor binding.

$$\mathrm{A} + \mathrm{R} \underset{k_-}{\overset{k_+}{\rightleftharpoons}} \mathrm{AR}$$

$$\mathrm{R} + \mathrm{AR} \underset{\psi_- k_-}{\overset{\psi_+ k_+}{\rightleftharpoons}} \mathrm{RAR}$$

The law of mass action gives rise to a system of ordinary differential equations (ODEs) that govern the binding kinetics of the reactions, namely:

$$\frac{d[R]}{dt} = -k_+[A][R] + k_-[AR] - \psi_+ k_+[R][AR] + \psi_- k_-[RAR], \tag{2.1a}$$

$$\frac{d[AR]}{dt} = k_+[A][R] - k_-[AR] - \psi_+ k_+[R][AR] + \psi_- k_-[RAR], \tag{2.1b}$$

$$\frac{d[RAR]}{dt} = \psi_+ k_+[R][AR] - \psi_- k_-[RAR]. \tag{2.1c}$$

with initial conditions

$$[R](0) = R_{tot}, \qquad [AR](0) = 0, \qquad [RAR](0) = 0, \tag{2.2}$$

where square brackets denote concentration, and all parameters and measured quantities are restricted positive. Here, R_{tot} is the total receptor concentration. We make the assumption that ligand is supplied in such a way that its concentration remains unchanged throughout any experiment (Lauffenburger and Linderman, 1993). The signal S of interest is proportional to the concentration of ligand-bound receptors (Kilpatrick et al., 2017), so we take

$$S = a([AR] + 2[RAR]), \tag{2.3}$$

where a is a scaling constant. Note that the signal contribution from one *RAR* complex, which contains two receptor protomers, is double that for one *AR* complex (see Kilpatrick et al., 2017). The total concentration of receptors is conserved, with

$$R_{tot} = [R] + [AR] + 2[RAR]. \tag{2.4}$$

$$\mathrm{A} + \mathrm{R} \underset{k_-}{\overset{k_+}{\rightleftharpoons}} \mathrm{AR}$$

$$\mathrm{R} + \mathrm{AR} \underset{\psi_- k_-}{\overset{\psi_+ k_+}{\rightleftharpoons}} \mathrm{RAR}$$

Fig. 2.2. Schematic representing the reactions resulting from the binding of a two poled ligand to two monomeric receptors.

We may use this to reduce the system (2.1) and eliminate one equation, leaving, for example

$$\frac{d[R]}{dt} = -\left(k_+[A] + \frac{\psi_- k_-}{2}\right)[R] + \left(k_- - \frac{\psi_- k_-}{2}\right)[AR] - \psi_+ k_+[R][AR] + \frac{\psi_- k_- R_{tot}}{2}, \tag{2.5a}$$

$$\frac{d[AR]}{dt} = \left(k_+[A] - \frac{\psi_- k_-}{2}\right)[R] - \left(k_- + \frac{\psi_- k_-}{2}\right)[AR] - \psi_+ k_+[R][AR] + \frac{\psi_- k_- R_{tot}}{2}. \tag{2.5b}$$

This reduced initial value problem has the initial conditions

$$[R](0) = R_{tot}, \quad [AR](0) = 0, \tag{2.5c}$$

with ligand introduced at time $t = 0$. Note that we assume there exists no constitutive dimerisation, hence dimers are solely ligand-induced. It is worth observing here that the current model is structurally similar to that of 'Model 1' in Alarcón and Page (2007). We now focus on an in-depth study of ligand binding and the induced dimerisation.

3. Equilibrium analysis

In the spirit of classical receptor theory, and in keeping with our previous work (White and Bridge, 2019), we first investigate the equilibrium behaviour of the system, in particular the effect of the equilibrium cooperativity factor $\psi = \psi_+/\psi_-$. The equilibrium relationships are

$$[AR] = K_A[A][R], \tag{3.1a}$$

$$[RAR] = \psi K_A[R][AR] = \psi K_A^2[A][R]^2, \tag{3.1b}$$

where $K_A = k_+/k_-$ is the equilibrium association constant (that is $K_A = 1/K_D$, where K_D is the usual dissociation constant). Combining with Eq. (2.4) gives equilibrium species in terms of parameters as

$$[R] = \frac{-(1 + K_A[A]) + \sqrt{(1 + K_A[A])^2 + 8\psi K_A^2[A]R_{tot}}}{4\psi K_A^2[A]}, \tag{3.2a}$$

$$[AR] = \frac{-(1 + K_A[A]) + \sqrt{(1 + K_A[A])^2 + 8\psi K_A^2[A]R_{tot}}}{4\psi K_A}, \tag{3.2b}$$

$$[RAR] = \frac{\left(1 + K_A[A] - \sqrt{(1 + K_A[A])^2 + 8\psi K_A^2[A]R_{tot}}\right)^2}{16\psi K_A^2[A]}. \tag{3.2c}$$

From (2.3), we then find the overall signal at equilibrium to be

$$S_{eq} = \frac{a\left(1 + K_A[A] + 4\psi K_A^2[A]R_{tot} - \sqrt{(1 + K_A[A])^2 + 8\psi K_A^2[A]R_{tot}}\right)}{4\psi K_A^2[A]}. \tag{3.3}$$

Letting $[A] \to \infty$ we see that $[R], [RAR] \to 0$, while $[AR], S_{eq} \to aR_{tot}$. This signal is a scaled concentration of the total bound ligand, hence is comparable to the total ligand bound expression in White and Bridge (2019); although there is similarity in the models, these expressions are very different. In White and Bridge (2019), the appearance of multiple inflections in the signal log dose–response (logDR) curve for pre-dimerised receptors is seen to be possible, for a range of binding cooperativity. We now consider the possibility of multiple inflections for the LID model.

Introducing a scaled signal

$$\widetilde{S}_{eq} = \frac{S_{eq}}{a},$$

we compute (symbolically in MATLAB Matlab, xxxx)

$$\frac{d^2\widetilde{S}_{eq}}{d\log_{10}[A]^2} = \frac{\log(10)^2\left(\frac{3K_A^2[A]^2+K_A^3[A]^3+3K_A[A]+12\psi K_A^2[A]R_{tot}+16\psi^2K_A^4[A]^2R_{tot}^2}{+8\psi K_A^3[A]^2R_{tot}+4\psi K_A^4[A]^3R_{tot}+1-\left((1+K_A[A])^2+8\psi K_A^2[A]R_{tot}\right)^{3/2}}\right)}{4\psi K_A^2[A]\left((1+K_A[A])^2+8\psi K_A^2[A]R_{tot}\right)^{3/2}}. \tag{3.4}$$

Possible inflections in the logDR curve occur when $[A]$ satisfies

$$\begin{aligned}&3K_A^2[A]^2+K_A^3[A]^3+3K_A[A]+12\psi K_A^2[A]R_{tot}+16\psi^2K_A^4[A]^2R_{tot}^2\\&+8\psi K_A^3[A]^2R_{tot}+4\psi K_A^4[A]^3R_{tot}+1\\&-\left((1+K_A[A])^2+8\psi K_A^2[A]R_{tot}\right)^{3/2}\\&=0,\end{aligned} \tag{3.5}$$

that is, when

$$\begin{aligned}&\left(3K_A^2[A]^2+K_A^3[A]^3+3K_A[A]+12\psi K_A^2[A]R_{tot}+16\psi^2K_A^4[A]^2R_{tot}^2\right.\\&\left.+8\psi K_A^3[A]^2R_{tot}+4\psi K_A^4[A]^3R_{tot}+1\right)^2\\&=\left((1+K_A[A])^2+8\psi K_A^2[A]R_{tot}\right)^3.\end{aligned} \tag{3.6}$$

Expanding and simplifying gives

$$\begin{aligned}&-8\psi K_A^3[A]^3R_{tot}(2\psi K_AR_{tot}+1)(K_A^4[A]^4+2K_A^3(4\psi K_AR_{tot}+1)[A]^3\\&+8\psi K_A^3R_{tot}(2\psi K_AR_{tot}+1)[A]^2-2K_A(4\psi K_AR_{tot}+1)[A]-1)=0.\end{aligned} \tag{3.7}$$

Nonzero values of $[A]$ which give possible inflections must therefore satisfy

$$\begin{aligned}&K_A^4[A]^4+2K_A^3(4\psi K_AR_{tot}+1)[A]^3+8\psi K_A^3R_{tot}(2\psi K_AR_{tot}+1)[A]^2\\&-2K_A(4\psi K_AR_{tot}+1)[A]-1\\&=0.\end{aligned} \tag{3.8}$$

We can quickly determine the number of positive roots for this quartic equation. Applying Descartes' Rule of Signs (Murray, 2007), since the sequence of coefficients in (3.8) contains only one sign change (as all parameters are positive), we find that the number of positive roots is exactly one. Therefore there is at most one inflection in the logDR curve for the signal given in (3.3). This is in contrast with the results found for pre-dimerised GPCRs (White and Bridge, 2019); multiple inflections ("multiphasic logDR curves") may be suggestive of pre-formed dimers but not of LID.

In Fig. 3.1 we show the effect of the equilibrium cooperativity factor ψ on the logDR relationship for the signal S and each of the receptor species. For each logDR curve for S, we note a single inflection point. Using Eq. (3.3), we find the EC_{50} value (the ligand concentration giving half-maximal signal) to be

$$EC_{50} = \frac{1}{K_A(1+\psi K_AR_{tot})}. \tag{3.9}$$

This expression notably differs from the EC_{50} expression for the linear pre-dimerised model (White and Bridge, 2019) in that it depends on R_{tot}. Furthermore, $[A] = EC_{50}$ is not a solution of (3.8), so we conclude that for this LID model the EC_{50} does not coincide exactly with an inflection in the logDR curve. We see in Fig. 3.1 that as ψ increases there is an approximate leftward shift in the overall signal, indicating a smaller EC_{50}. Inspection of the individual species curves gives further insights.

For high cooperativity, with low ligand concentration, the signal is dominated by the contribution from RAR dimers, and $S \approx 2a[RAR]$. For high ligand concentration, the system becomes saturated with ligand as $[A]$ increases, leading to a decrease in $[RAR]$ as the availability of receptor monomers for dimerisation drops off. A plateau in the logDR curve for $[RAR]$ is clear. We see that the overall signal reaches saturation at a much lower concentration of A than $[AR]$ does.

With low cooperativity, the decreased propensity for dimerisation results in lower concentrations of $[A]$ being required for the same increase in bound monomers than when cooperativity is high. Only a small proportion of ligand-bound monomers bind a second receptor, causing dimerisation. Hence the signal increases largely with monomeric bound receptors. Interestingly we see that the peak in $[RAR]$ appears to be at the same level of $[A]$ regardless of

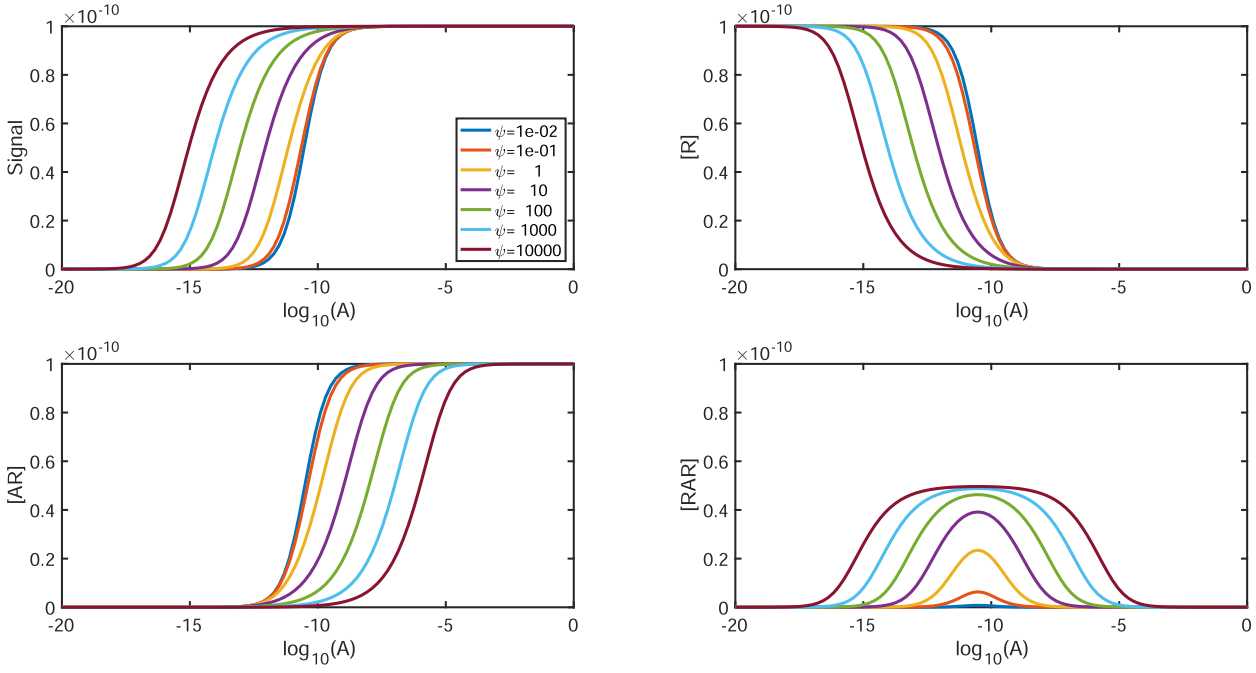

Fig. 3.1. LogDR curves for varying cooperativity factor, ψ. The plots show the overall signal as well as concentrations of R (Eq. (3.2a)), AR (Eq. (3.2b)) and RAR (Eq. (3.2c)). Base parameter values for the plot can be found in Appendix A.

the cooperativity value. To find this value, we first compute the derivative of $[RAR]([A])$ (using (3.2c)):

$$\frac{d[RAR]}{d[A]} = \frac{(1-K_A[A])\left(1+K_A[A]-\sqrt{(1+K_A[A])^2+8\psi K_A^2[A]R_{tot}}\right)^2}{16\psi K_A^2[A]^2\sqrt{(1+K_A[A])^2+8\psi K_A^2[A]R_{tot}}}. \tag{3.10}$$

The positive critical point is given by

$$[A] = \frac{1}{K_A}. \tag{3.11}$$

That is, the location of the critical point is independent of ψ, and is equal to the equilibrium dissociation constant, K_D. Hence this peak will appear to some extent regardless of the cooperativity levels. The corresponding value of $[RAR]$ depends on the cooperativity factor ψ, and is given by

$$[RAR]|_{\frac{1}{K_A}} = \frac{\left(1-\sqrt{1+2\psi K_A R_{tot}}\right)^2}{4\psi K_A}. \tag{3.12}$$

It is apparent from Fig. 3.1 that as $\psi \to \infty$, the maximum value of $[RAR]|_{\frac{1}{K_A}}$. tends to a limit. From (3.12), we see that

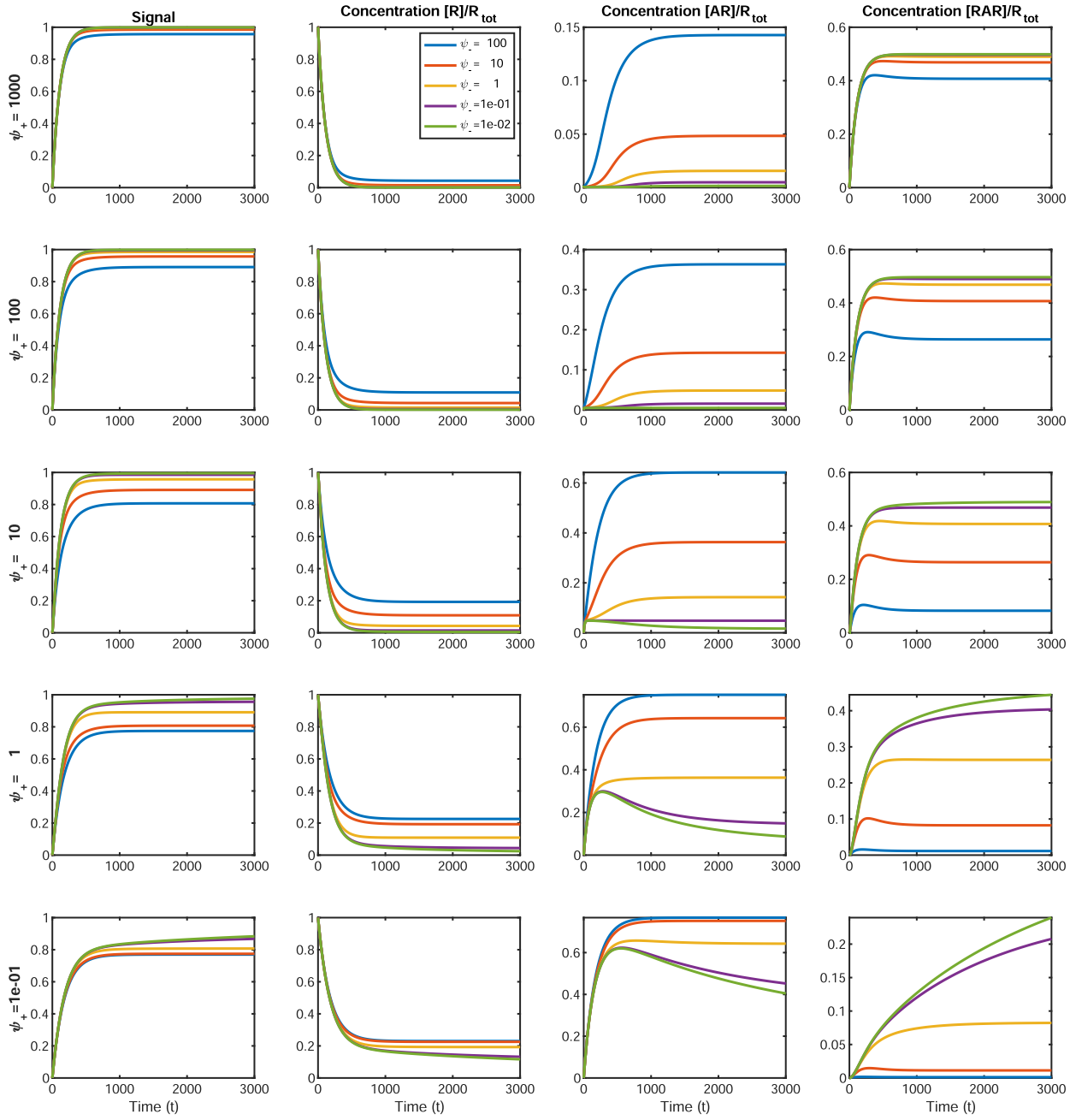

Fig. 4.1. A numerical investigation into the effects of cooperativity factors ψ_+ and ψ_- on dynamics. The columns show the overall signal as well as individual species (Equations. (2.1)) while in each row we fix the ψ_+ value. Each plot then shows a results for varying ψ_-. Plots are created with ligand concentration $[A] = 10^{-10}M$.

$$[RAR]|_{\frac{1}{K_A}} \to \frac{R_{tot}}{2} \qquad \text{as } \psi \to \infty. \tag{3.13}$$

4. Binding dynamics - numerical simulations

In Fig. 4.1, we present numerical results to show how kinetic cooperativity factors affect the binding dynamics of individual species and the resulting overall signal. The lefth-hand column shows the signal S as we increase ψ_+ from top to bottom. In the second, third and fourth columns, we plot $[R], [AR]$ and $[RAR]$ respectively. In each plot, we also vary ψ_-. We fix k_+ and k_-, within the range of reported binding affinities (Mac Gabhann and Popel, 2007 and references within), to allow us to focus on the effects that cooperativity factors ψ_+ and ψ_- have on the binding dynamics. Parameter values used to create the plot can be seen in Appendix A.

First looking at the overall signal S (in the first column), we notice that increasing ψ_+ leads to a larger signal at equilibrium. Increasing ψ_+ gives an increased rate of binding of a second monomer, and so the larger signal comes from higher $[RAR]$. Similarly, decreasing ψ_- gives an increase in the equilibrium signal. As ψ_- decreases, the time taken to reach equilibrium is also increased. The individual species timecourses give further insights.

When ψ_- is small (slowed dimer dissociation rate), we see peaks in the $[AR]$ curves. Ligand-bound monomeric receptors dimerise but have low propensity for undimerising, and the concentration of bound monomers falls. The low undimerisation rate also explains the extended time for the system to reach equilibrium. Conversely, if ψ_- is large, peaks appear instead in the dimer concentration, $[RAR]$. Ligands bind monomers which in turn form dimers. However, with an increased dimer dissociation rate these quickly return back to monomers, and so we see a peak in the $[RAR]$ timecourse.

For large ψ_+, we note an initial rapid increase in $[AR]$, followed by an approach to equilibrium on a much longer timescale. The large forward cooperativity factor results in rapid dimerisation of ligand-bound monomers, and hence fewer free monomeric receptors, which keeps $[AR]$ low. Exact solutions to (2.1) are not available to give further insights and results, but in Section 5, we use asymptotic analysis to find approximate solutions for certain parameter regimes.

5. Asymptotic analysis

5.1. Dimensionless equations

In order to analyse the system asymptotically we first cast the initial value problem (2.1) in dimensionless form. We let

$$[R] = R_{tot} r, \quad [AR] = \alpha R_{tot} p, \quad [RAR] = \frac{\alpha^2 \beta R_{tot}}{\gamma} q, \quad t = \frac{1}{k_-}\tilde{t}, \tag{5.1}$$

where

$$\alpha = K_A[A], \quad \beta = \frac{\psi_+ R_{tot}}{[A]}, \quad \gamma = \psi_-, \tag{5.2}$$

The governing system (2.1) then gives the dimensionless system

$$\frac{dr}{d\tilde{t}} = \alpha(p - r) + \alpha^2\beta(q - rp), \tag{5.3a}$$

$$\frac{dp}{d\tilde{t}} = r - p + \alpha\beta(q - rp), \tag{5.3b}$$

$$\frac{dq}{d\tilde{t}} = \gamma(pr - q), \tag{5.3c}$$

with initial conditions

$$r(0) = 1, \qquad p(0) = 0, \qquad q(0) = 0. \tag{5.4}$$

Alternatively, we can use the nondimensionalised version of the reduced system (2.5), namely:

$$\frac{dr}{d\tilde{t}} = -\left(\alpha + \frac{\gamma}{2}\right)r + \left(1 - \frac{\gamma}{2}\right)\alpha p - \alpha^2\beta rp + \frac{\gamma}{2}, \tag{5.5a}$$

$$\frac{dp}{d\tilde{t}} = \left(1 - \frac{\gamma}{2\alpha}\right)r - \left(1 + \frac{\gamma}{2}\right)p - \alpha\beta rp + \frac{\gamma}{2\alpha}, \tag{5.5b}$$

with initial conditions

$$r(0) = 1, \quad p(0) = 0, \tag{5.5c}$$

Conservation of receptor (2.4) now reads

$$1 = r + \alpha p + \frac{2\alpha^2\beta}{\gamma} q, \tag{5.6}$$

which can be used to determine the concentration of q where necessary. Full details of the nondimensionalisation calculations are given in Appendix B.

Biologically, α is the ligand concentration scaled by equilibrium dissociation rate, so $\alpha \gg 1$ if either the ligand concentration is very high or has a very high affinity. The parameter β depends on the cooperativity factor ψ_+ as well as the total ligand-receptor concentration ratio. So $\beta \gg 1$ may correspond to large ψ_+, which gives an increased rate at which dimers are formed. Also, $\beta \gg 1$ may correspond to overexpression of receptor. As γ is simply the parameter ψ_-, if $\gamma \gg 1$ then we have fast dimer dissociation compared with monomeric receptor dissociation. The equilibrium solutions for this dimensionless system are

$$r^{eq} = p^{eq} = \frac{\gamma\left(-(1+\alpha) + \sqrt{(1+\alpha)^2 + 8\frac{\alpha^2\beta}{\gamma}}\right)}{4\alpha^2\beta}, \qquad q^{eq} = (r^{eq})^2. \tag{5.7}$$

5.2. Asymptotic approximations

In the numerical results of Section 4 we saw that small ψ_- leads to a peak in the $[AR](t)$ curve, whilst large ψ_- leads to a peak instead in $[RAR](t)$. Also, large ψ_+ gives a rapid increase in $[AR](t)$. To investigate such behaviour further, we now consider asymptotic regimes for the three nondimensional parameters α, β and γ in Equations. (5.5) (where we drop the tilde on t for simplicity). We consider three parameter regimes corresponding to dimerisation behaviour of interest. Binding rates of VEGF are well documented (Mac Gabhann and Popel, 2007 and references within); throughout this section we assume $\alpha = O(1)$, allowing us to focus on the possible effects of *cooperativity*.

5.3. Small backwards cooperativity (γ) asymptotics - slow dimer dissociation

In Fig. 4.1 we saw that slow dimer dissociation rate gave a peak in $[AR](t)$. Slow dimer dissociation corresponds to small γ in the dimensionless system, so we set $\gamma = \epsilon$, where $0 < \epsilon \ll 1$. Substituting this into (5.5) gives

$$\frac{dr}{dt} = -\left(\alpha + \frac{\epsilon}{2}\right)r + \left(1 - \frac{\epsilon}{2}\right)\alpha p - \alpha^2\beta rp + \frac{\epsilon}{2}, \tag{5.8a}$$

$$\frac{dp}{dt} = \left(1 - \frac{\epsilon}{2\alpha}\right)r - \left(1 + \frac{\epsilon}{2}\right)p - \alpha\beta rp + \frac{\epsilon}{2\alpha}, \tag{5.8b}$$

where conservation of receptor (5.6) gives

$$q = \frac{\epsilon}{2\alpha^2\beta}(1 - r - \alpha p) \tag{5.8c}$$

This is a regularly perturbed problem. Assuming asymptotic approximations

$$r \approx r_0 + \epsilon r_1 + \ldots, \quad p \approx p_0 + \epsilon p_1 + \ldots, \tag{5.9}$$

where each r_i, p_i is $O(1)$, and substituting these into Equations. (5.8) gives the leading order problem as

$$\frac{dr_0}{dt} = -\alpha r_0 + \alpha p_0 - \alpha^2 \beta r_0 p_0, \tag{5.10a}$$

$$\frac{dp_0}{dt} = r_0 - p_0 - \alpha\beta r_0 p_0, \tag{5.10b}$$

$$r(0) = 1, \quad p(0) = 0, \tag{5.10c}$$

Although this is still a nonlinear system that we are not able to solve analytically, we can make some observations. The terms that remain in the ODEs include the linear terms, representing the reversible binding of ligand to monomeric receptor, as well as the nonlinear term representing forward dimerisation. Terms representing the dissociation of dimers do not appear in the reduced system (5.10). So as receptors dimerise, they become "stuck" in this form, with the concentration of dimers increasing monotonically. In Fig. 5.1 we plot a typical solution of the full nondimensional system (5.8), along with the solution of the corresponding approximate system (5.10). We see little difference in the two solutions; neglecting the terms in the approximate solution has little effect on the overall dynamics.

5.4. Large β asymptotics (fast dimerisation)

Another feature appearing in Fig. 4.1 is that when ψ_+ is large, we see a rapid initial increase in $[AR](t)$, followed by approach to equilibrium on a longer timescales. To gain further insights for the case of fast dimerisation (large ψ_+, giving large β), we set $\beta = 1/\epsilon$, where $0 < \epsilon \ll 1$. Then the system (5.3) becomes

$$\epsilon \frac{dr}{dt} = \epsilon\alpha(p - r) + \alpha^2(q - rp), \tag{5.11a}$$

$$\epsilon \frac{dp}{dt} = \epsilon(r - p) + \alpha(q - rp), \tag{5.11b}$$

$$\frac{dq}{dt} = \gamma(pr - q), \tag{5.11c}$$

with initial conditions

$$r(0) = 1, \qquad p(0) = 0, \qquad q(0) = 0. \tag{5.11d}$$

We have a singularly perturbed problem; the asymptotic analysis here will elucidate the multiple timescales which govern the dynamics. Full details of the analysis are given in Appendix C.

The first timescale of interest is $t = O(\epsilon)$, which gives an *inner* or *initial* layer. The leading-order approximation to the solution of (5.11) in this layer is found to be (see Appendix C.2):

$$r(t) \equiv 1, \qquad p(t) = \epsilon\left(\frac{1 - e^{-\frac{\alpha t}{\epsilon}}}{\alpha}\right), \qquad q(t) = \epsilon^2 \frac{\gamma}{\alpha^2}\left(\frac{\alpha t}{\epsilon} - 1 + e^{-\frac{\alpha t}{\epsilon}}\right). \tag{5.12}$$

Note that the solutions $r(t)$ and $p(t)$ are independent of γ. Biologically, the solution $p(t)$ corresponds to monoexponential ligand-monomeric receptor binding kinetics. We note that $p(t)$ depends on α, which controls binding kinetics but not dimerisation. This binding phase is confined to the short timescale $t = O(\epsilon)$, beyond which the effect of large dimerisation rate is seen. On this short timescale, the kinetics of q are driven by forward dimerisation only (as seen by the terms which remain in the reduced ODE system (C.10)).

The next timescale that we consider is $t = O(1)$, under an intermediate scaling of the dependent variables with $r = O(1), p = O(\epsilon)$ and $q = O(\epsilon)$. The approximate solutions of (5.11) in this region are (see the analysis in Appendix C.3):

$$r(t) = e^{-2\alpha t}, \qquad p(t) = \epsilon\left(\frac{1}{\alpha} + \frac{\gamma}{2\alpha^2}\left(e^{2\alpha t} - 1\right)\right), \qquad q(t) = \frac{\epsilon\gamma}{2\alpha^2}\left(1 - e^{-2\alpha t}\right). \tag{5.13}$$

As the parameter γ appears in this solution we can see that as we move into this region the second reaction, whereby the ligand binds a second monomer, now also plays a role in the dynamics of the system. The observed decay constant of the receptor concentration, 2α, is due to both free ligand and receptor-bound ligand binding available monomeric receptors. Also, we note the exponential growth and decay terms in the solution on this timescale. These intermediate solutions are valid in an "overlap" region, where they agree with the outer solutions, which capture the approach to equilibrium.

The final approximate solution we consider, namely the outer solution, has $t = O(1)$ with $r = O\left(\epsilon^{\frac{1}{2}}\right), p = O\left(\epsilon^{\frac{1}{2}}\right)$ and $q = O(\epsilon)$. We find that the approximate solution of (5.11) in this outer region has $r(t)$ given implicitly by (see Appendix C.4):

$$\log\left(\epsilon^{-\frac{1}{2}} r(t)\right) - \frac{(\alpha + 1)\log|\gamma - 2\alpha^2\epsilon^{-1}r^2(t)|}{2\alpha} = 2t + c_1, \qquad c_1 = \frac{1}{2\alpha}\log\frac{\epsilon}{(2\alpha^2)^{\alpha+1}}, \tag{5.14}$$

and $p(t)$ and $q(t)$ given by

$$p(t) = \epsilon\frac{\gamma}{2\alpha^2 r(t)}, \qquad q(t) \equiv \epsilon\frac{\gamma}{2\alpha^2}. \tag{5.15}$$

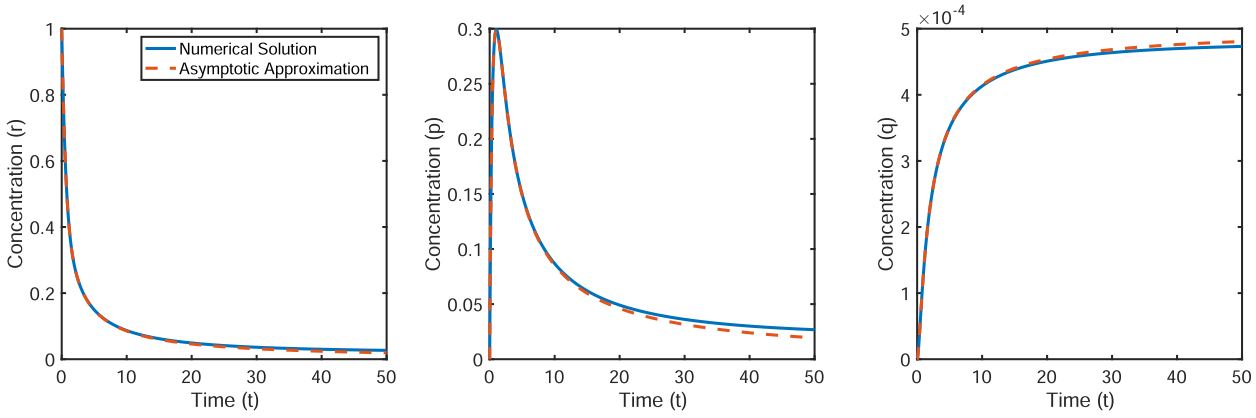

Fig. 5.1. Both the solution to the full system in Equations. (5.8) is plotted along side the solution of the reduced, approximated system (Equations. (5.10)) in red. Conservation of receptors is used to show the approximation for q. Parameters used to create plots are $\alpha = \beta = 1$ and $\gamma = \epsilon = 0.001$.

Biologically, reversible dimerisation is in approximate equilibrium in this outer region, with all species approaching their steady-state concentrations. All of the approximate solutions now depend on both α and γ, and we conclude that on this final timescale, both reactions (ligand binding monomer receptor, and dimerisation) now affect all concentrations.

Fig. 5.2 shows an example numerical computation. We see a good match between the intermediate solution and both the inner and outer solutions for all variables, and together the approximations agree with the numerics in each region.

5.5. Large γ asymptotics

The last case we consider is when we have fast dimer dissociation, that is when γ is large. In Fig. 4.1 we saw that taking ψ_-, and hence $\gamma = \psi_-$, large caused a peak in the bound dimer, $[RAR](t)$, curve. As such we set $\gamma = 1/\epsilon$, with $0 < \epsilon \ll 1$. Then the system (5.3) gives

$$\frac{dr}{dt} = \alpha(p - r) + \alpha^2\beta(q - rp), \tag{5.16a}$$

$$\frac{dp}{dt} = r - p + \alpha\beta(q - rp), \tag{5.16b}$$

$$\epsilon\frac{dq}{dt} = pr - q, \tag{5.16c}$$

with initial conditions

$$r(0) = 1, \qquad p(0) = 0, \qquad q(0) = 0. \tag{5.17}$$

Again we find a singular perturbation problem, indicating multiple time scales that contribute to the dynamics. Full details of the analysis can be found in Appendix D. We consider the solution over different timescales, and only state the results here.

We first consider an inner region, where $t = O(\epsilon)$, and in which $r = O(1), p = O(\epsilon)$ and $q = O(\epsilon)$. The leading order approximate solution to (5.16) in this region is found to be (see Appendix D.2):

$$r(t) \equiv 1, \qquad p(t) = t, \qquad q(t) = t + \epsilon\left(e^{-\frac{t}{\epsilon}} - 1\right). \tag{5.18}$$

Biologically, the dominant reactions on this timescale are the forward binding of ligand to monomeric receptor, which only affects AR dynamics, and the reversible dimerisation.

In the outer region, in which $t = O(1), r = O(1), p = O(1)$ and $q = O(1)$, the leading order approximate solutions to (5.16) are given by (see Appendix D.3):

$$r(t) = \frac{1+\alpha e^{-(\alpha+1)t}}{1+\alpha}, \qquad p(t) = \frac{1-e^{-(\alpha+1)t}}{1+\alpha},$$
$$q(t) = \frac{1+(\alpha-1)e^{-(\alpha+1)t} - \alpha e^{-2(\alpha+1)t}}{(1+\alpha)^2}. \tag{5.19}$$

Biologically, the dominant reactions on this timescale are the reversible binding of ligand to monomeric receptor, while reversible dimerisation has approximately reached equilibrium due to the rapid undimerisation. Any receptors in dimerised form quickly return to monomeric state. The outer solution for $q(t)$ in (5.19) gives an approximate condition for, and location of, the observed peak in $q(t)$. We calculate

$$\frac{dq(t)}{dt} = \frac{-e^{-2(\alpha+1)t}\left(2\alpha + e^{(\alpha+1)t} - \alpha e^{(\alpha+1)t}\right)}{\alpha+1}. \tag{5.20}$$

Equating this derivative to zero, we find that a stationary point for $q(t)$ is located at

$$t_s = \frac{\log\left(\frac{2\alpha}{\alpha-1}\right)}{\alpha+1}, \tag{5.21}$$

for $\alpha > 1$. A peak appears for $\alpha > 1$, that is, for the scaled ligand concentration greater than unity.

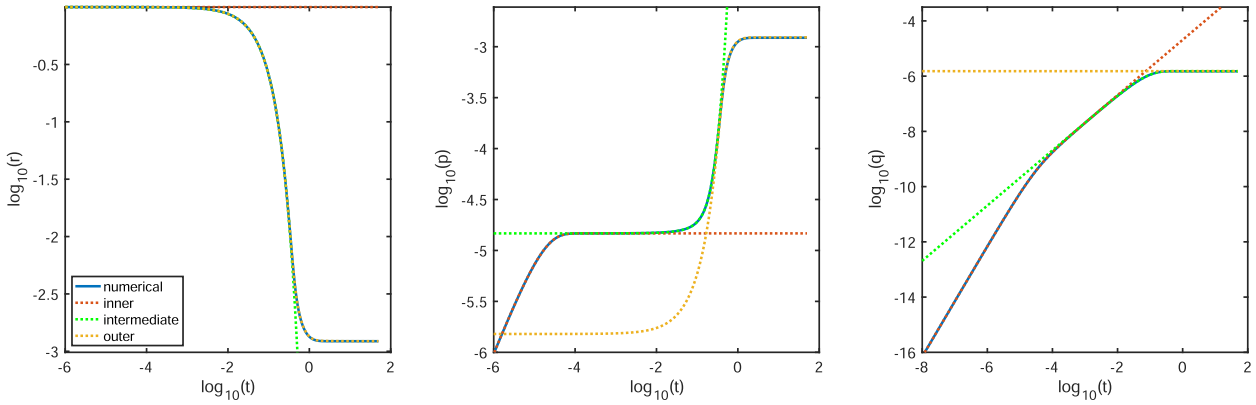

Fig. 5.2. Numerical solution of Equation. (5.11) with inner (Eq. (5.12)), intermediate (Eq. (5.13)) and outer (Eqs. (5.14) and (5.15)) solutions, on a log–log scale. The intermediate solution matches both the inner and outer solution, creating a full approximation to the numerical solution. Conservation of receptors is used to show the approximation for q. Plot created with $\alpha = 6.8, \gamma = 1.4$ and $\beta = \epsilon = 10^{-4}$.

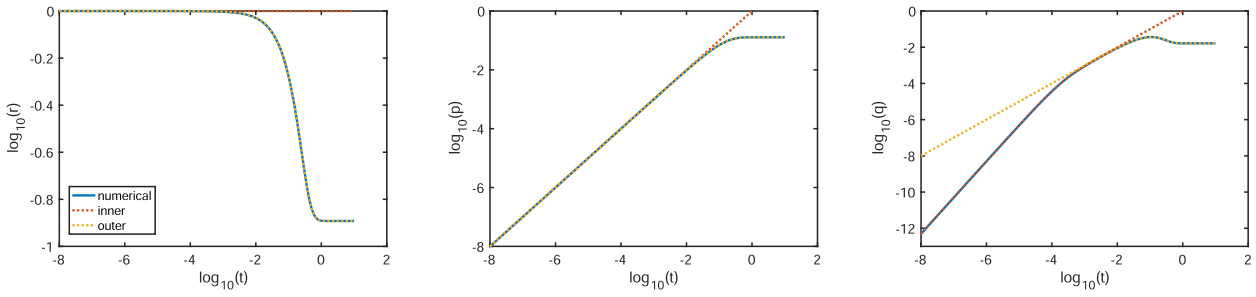

Fig. 5.3. The numerical solution of Equation. (5.16) with asymptotic solutions (5.18) and (5.19) on a log–log scale, showing good agreement in both regions. Parameters used to create plot are α=6.8, β=1, $\epsilon = 10^{-4}$.

In Fig. 5.3 we see a good match between the inner and outer solution in all curves. We also see good agreement between the approximate solution and the numerical solutions in both regions.

6. Model validation

Here we present a preliminary validation of our model by fitting numerical solutions of the system (2.1)–(2.3) to published experimental data in the form of timecourses corresponding to the signal $S(t)$ defined in (2.3), in response to three ligands over a range of concentrations. Raw data were kindly provided by Dr. Chloe Peach (P. communication between Lloyd Bridge, 2019). In Peach et al. (2019), three VEGF-A isoforms ($VEGF_{165}$a-TMR, $VEGF_{165}$b-TMR and $VEGF_{121}$a-TMR) are each supplied to cells or membranes, over a range of five concentrations, and the "binding signal" corresponding to $S(t)$ (ligand bound to VEGFR2) is measured using bioluminescence resonance energy transfer (BRET). While experiments are performed using both HEK293T intact cells and membranes, we focus only on membrane results, thus reducing the possibility of data being affected by other processes such as receptor internalisation which may cause a reduction in signal on longer time scales.

For each of the three ligands, the sum of the squared differences between the simulation results and the experimental data, across all time points for all five concentrations, is minimised. The optimisation is performed in Copasi (Hoops et al., 2006) using a particle swarm optimization method, with a swarm size of 100 and 3000 iterations. For each ligand, the five timecourses are fitted to simultaneously, and estimates for $a, R_{tot}, k_+, k_-, \psi_+$ and ψ_- are found. We note that it is reasonable to expect the underlying values of a, which is an experimental scaling factor, and R_{tot} to be close across all experiments since the experimental conditions will be controlled and membrane preparations with similar receptor numbers are to be expected. We indeed see order-of-magnitude agreement in these two parameters across all estimates shown in Table 6.1. An alternative approach to parameter estimation assuming these two parameters to be equal across all experiments is possible; an illustrative result is shown in Fig. E.1 and Table E.1.

In Table 6.1 we show the parameter estimates returned from fitting, while in Fig. 6.1 we plot the fitted curves together with the data. Clearly the estimates give an excellent fit to all data sets. Looking at the estimated parameter values, we also note that all association and dissociation kinetic rate constants fall into the previously reported ranges (Mac Gabhann and Popel, 2007) (and references within), and agree within order-of-magnitude with the simulation parameters listed in Table A.1.

In all cases, we have $\psi_+ > \psi_-$ and, therefore, positive equilibrium cooperativity. Comparing our estimates with those presented in Peach et al. (2019), where the data were fitted to a simple monomeric binding model, we see our estimated k_+ values are consistently lower than in Peach et al. (2019), and our k_- values are consistently higher, but within order-of-magnitude. Our rank-order for the association rates is in agreement with (Peach et al., 2019), with $VEGF_{165}$a-TMR having the highest k_+, and $VEGF_{121}$a-TMR having the lowest. Differences in these parameter values across the two studies are to be expected, of course, since the process of LID is not modelled in (Peach et al., 2019).

To further understand the implications of these estimations we plot the individual species curves for all results in Fig. 6.2. We note the appearance of peaks in some of the $[RAR](t)$ curves. In particular, these appear for the higher ligand concentrations of the $VEGF_{165}$a-TMR and $VEGF_{121}$a-TMR curves. In Table 6.2 we consider the nondimensional parameter values for the estimated parameters. For each ligand, our estimates correspond to large β and large γ, which were studied independently as asymptotic cases in Section 5, where it was assumed that $\alpha = O(1)$ (which our estimates yield for moderate to high ligand concentration). Peaks in $[RAR]$ are observed in 6.2 for high ligand concentration (with $\alpha > 1$) for isoforms $VEGF_{165}$a-TMR and $VEGF_{121}$a-TMR, as in (5.21) where

Table 6.1
Estimated parameters returned from fitting to the data, as seen in Fig. 6.1. Units: k_+ (M^{-1} min^{-1}), k_- (min_{-1}), R_{tot} (M).

	a	k_+	k_-	ψ_+	ψ_-	R_{tot}
$VEGF_{165}$a-TMR	1.71×10^7	5.78×10^6	4.60×10^{-2}	3.11×10^3	1.79×10^3	6.19×10^{-9}
$VEGF_{165}$b-TMR	5.04×10^7	1.61×10^6	6.58×10^{-2}	2.31×10^4	5.05×10^2	1.87×10^{-9}
$VEGF_{121}$a-TMR	1.64×10^7	3.08×10^6	2.45×10^{-2}	6.51×10^3	4.97×10^3	5.35×10^{-9}

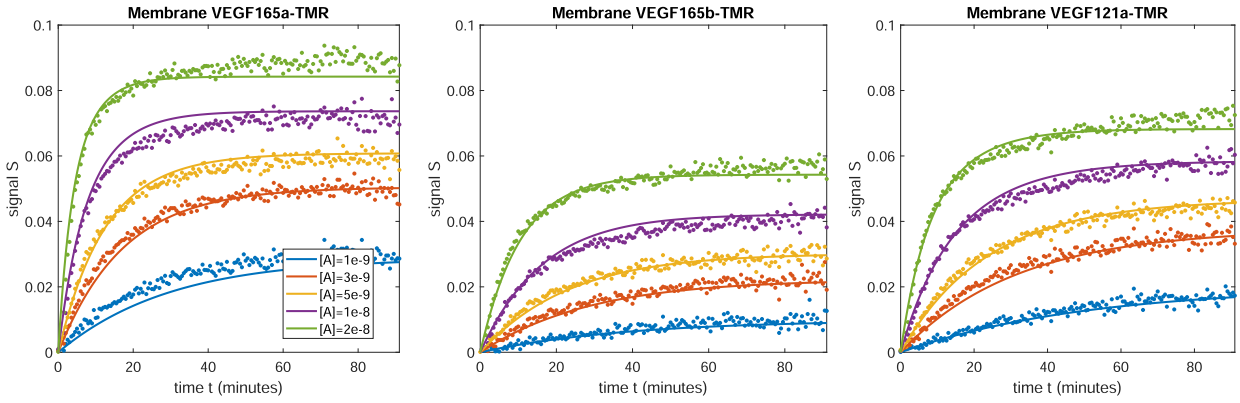

Fig. 6.1. Data published in Peach et al. (2019) are used to estimate the model parameters. Experiments were performed using five concentrations of three different VEGF isoforms (VEGF $_{165}$a-TMR, VEGF $_{165}$b-TMR and VEGF $_{121}$a-TMR) and the signal $S(t)$ (2.3) is recorded. An excellent fit to the data is seen from fitting to all data sets individually. Parameter values returned can be seen in Table 6.1.

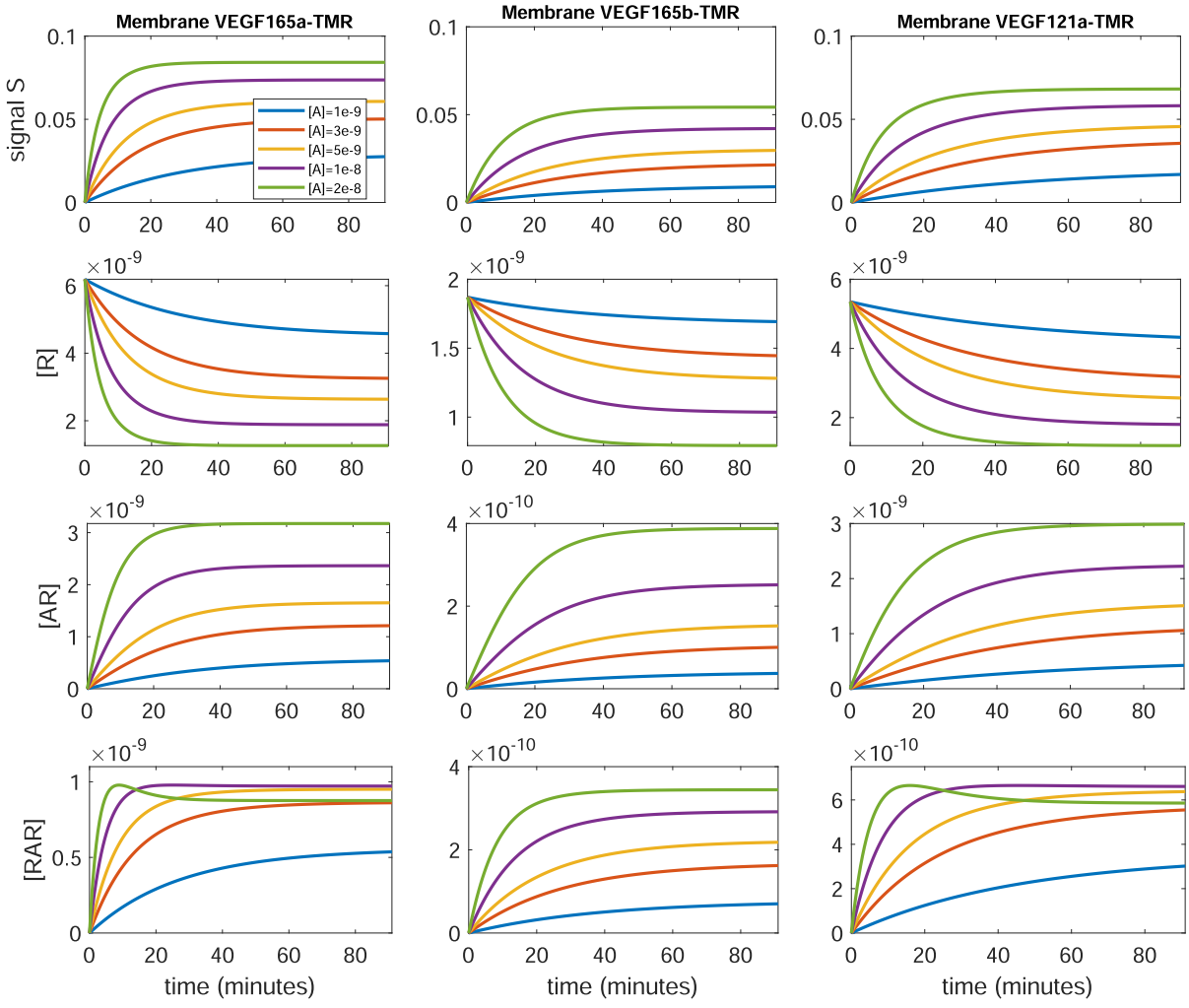

Fig. 6.2. Individual species curves and signal timecourses (numerical solutions to (2.1)–(2.3)) using the estimated parameters from Table 6.1 show peaks in some of the $[R.AR](t)$ curves.

we considered $\alpha = O(1)$ and $\gamma \gg 1$. Further, we note that the monotonic nature of the measured signal S versus ligand concentration relationship at all time points is not always replicated in the $[RAR]$ versus concentration curves. Given the potential differential roles and kinetic rates associated with AR and RAR in signalling (Mac Gabhann and Popel, 2007) and internalisation (Kilpatrick et al., 2017), and that the interaction of RAR with other species is of significant biological importance (Mac Gabhann and Popel, 2007), it is clear that being able to parameterise the LID process in terms of binding cooperativity may be potentially important towards functional studies and more detailed signalling and systems biology models (Mac Gabhann et al., 2010). As noted in Mac Gabhann et al. (2010); Mac Gabhann and Popel (2004), different receptor combinations (including those modelled by AR and RAR here) may differentially activate a number of alternate signalling pathways. The development of VEGF-targeted therapies will benefit from quantitative understanding of the range of potential binding dynamics at the top of these pathways.

Table 6.2
Nondimensional parameter combinations with estimated parameters, taking $[A] = 5 \times 10^{-9}$ as a representative value in the middle of the range considered.

	$VEGF_{165}$a-TMR	$VEGF_{165}$b-TMR	$VEGF_{121}$a-TMR
$\alpha = K_A[A]$	0.628	0.122	0.629
$\beta = \psi_+ R_{tot}/[A]$	3850	8639	6965
$\gamma = \psi_-$	1790	505	4970

7. Discussion

We have presented a model for the dynamics of ligand-induced dimerisation (LID), with specific reference to the binding of VEGF to VEGFRs. This work represents an in-depth mathematical analysis of the binding kinetics which have been considered partially in earlier models (Mac Gabhann and Popel, 2007;Alarcón and Page, 2007). This detailed analysis has resulted in an elucidation of the potential dynamics in response to a range of model parameters. In particular, new analytical expressions for equilibrium responses provide a simple, powerful platform for the analysis of systems

exhibiting LID. An interesting feature of the expressions for equilibrium binding is that log-dose–response (logDR) curves will not contain multiple inflections for LID, in contrast with the analagous results for ligands binding pre-dimerised GPCRs (White and Bridge, 2019). Hence the existence of multiphasic logDR curves with multiple inflections is not an indicator of LID.

A significant advance over equilibrium studies (even where ODE models have been formulated Mac Gabhann and Popel, 2007) is the analysis of ligand binding dynamics for LID. While a purely pre-dimerised receptor model results in a linear model which can be solved exactly via eigenvalue analysis or Laplace Transforms (White and Bridge, 2019), the corresponding LID model considered here is significantly more challenging to solve. The nonlinear nature of the ODE system requires numerical solutions. Numerical simulations have provided insights into the signalling dynamics by considering a modelled signal corresponding to experimental data (Peach et al., 2019), while asymptotic analysis has been used to provide insights into the key dominant reaction sequences over multiple timescales, and exact solutions for particular parameter regimes. The analysis presented here extends both our understanding of the potential dynamics of the LID system, and the "mathematical pharmacology" literature in receptor theory (Bridge, 2009; Bridge et al., 2010; Woodroffe et al., 2009; Peletier and Gabrielsson, 2018; van der Graaf et al., 2016).

We validate our model by fitting to recent published, experimental data, where we see that the model gives an excellent fit to the data across all curves. This gives confidence that the model may accurately describe the binding and dimerisation processes for the VEGF-VEGFR system, and may be used to estimate pharmacologically relevant kinetic parameters.

A key next step in our work will be the application of structural identifiability analysis (SIA) to our ODE model in order to determine which parameters are theoretically estimable from a given model readout. Compared to many systems biology ODE models, our LID model is low-dimensional. Even so, SIA is challenging. For low-dimensional linear models, SIA results may be obtained via relatively straightforward transfer function methods (Grewal and Glover, 1976; Godfrey and DiStefano, 1985; Janzén et al., 2016), but the nonlinear LID model will require series solution or transformation methods (Janzén et al., 2016; Pohjanpalo, 1978; Chis et al., 2011). While SIA is often used in pharmacokinetic studies, its use in receptor theory kinetic models is sparse. We propose a comparative study of SIA applied to ligand binding models for both pre-dimerised and ligand-induced dimers.

Finally, given the apparent excellent fit of our model to recent experimental data for non-internalising VEGF receptors, we propose as future work an extension of the current model to incorporate the internalisation of VEGFR which has also been observed in recent experiments (Peach et al., 2018; Peach et al., 2019; Kilpatrick et al., 2017). Further analysis, quantification of binding and internalisation rates, and simulation will contribute to the literature on VEGFR and its associated signalling pathways of biomedical interest.

Author contributions

All authors devised the project, developed models, performed analysis and computation, and wrote the manuscript.

Declaration of Competing Interest

The authors declare that they have no known competing financial interests or personal relationships that could have appeared to influence the work reported in this paper.

Table A.1
Values used for plotting are taken from Mac Gabhann and Popel (2007).

Parameter	R_{tot}	k_+	k_-	K_A
Value	$2\times10^{-10}M$	$4.4\times10^{7}M^{-1}s^{-1}$	$1.32\times10^{-3}s^{-1}$	$3.3\times10^{10}M^{-1}$

Acknowledgements

We thank Professor Steve Hill and Dr. Laura Kilpatrick (University of Nottingham) and Dr. Chloe Peach (New York University) for helpful discussions regarding modelling the LID system and fitting data. Dr. Gibin Powathil (Swansea University) gave supervisory support to CW.CW was supported by a College of Science PhD studentship at Swansea University. LB was supported in part by a Faculty of Environment and Technology funding award at UWE Bristol.

Appendix A. Parameter values

In this appendix, we give parameter values used for simulations. The values were taken from ranges reported in Mac Gabhann and Popel (2007) (and references within) and can be seen in Table A.1.

Appendix B. Nondimensionalisation

We consider the nondimensionalisation of Equations. (2.1). We let the dimensionless free receptor r be given by

$$[R] = R_{tot}r \qquad \Rightarrow\ r = \frac{[R]}{R_{tot}}. \tag{B.1}$$

To scale $[AR]$ and $[RAR]$ we first recall the equilibrium concentrations

$$[AR] = K_A[A][R], \qquad [RAR] = \psi K_A[R][AR] = \psi K_A^2[A][R]^2, \tag{B.2}$$

We use these to give us scalings for $[AR]$ and $[RAR]$ as

$$[AR] = K_A[A]R_{tot}p \qquad \Rightarrow\ p = \frac{[AR]}{K_A[A]R_{tot}}, \tag{B.3}$$

$$[RAR] = \psi K_A^2[A]R_{tot}^2 q \qquad \Rightarrow\ q = \frac{[RAR]}{\psi K_A^2[A]R_{tot}^2}, \tag{B.4}$$

where p and q are the new nondimensional single-bound receptor and dimerised receptor, respectively. Finally, we set

$$t = \frac{\tilde{t}}{k_-} \qquad \Rightarrow\ \tilde{t} = k_- t. \tag{B.5}$$

The original system (2.1) then gives the dimensionless system

$$\frac{dr}{d\tilde{t}} = \alpha(p - r) + \alpha^2\beta(q - rp), \tag{B.6a}$$

$$\frac{dp}{d\tilde{t}} = r - p + \alpha\beta(q - rp), \tag{B.6b}$$

$$\frac{dq}{d\tilde{t}} = \gamma(pr - q), \tag{B.6c}$$

where

$$\alpha = K_A[A], \quad \beta = \frac{\psi_+ R_{tot}}{[A]}, \quad \gamma = \psi_-, \tag{B.7}$$

with initial conditions

$$r(0) = 1, \qquad p(0) = 0, \qquad q(0) = 0. \tag{B.8}$$

Conservation of receptor now reads

$$1 = r + \alpha p + \frac{2\alpha^2\beta}{\gamma}q, \tag{B.9}$$

which gives an expression for q:

$$q = \frac{\gamma}{2\alpha^2\beta}(1 - r - \alpha p). \tag{B.10}$$

Alternatively, the reduced system (2.5) gives

$$\frac{dr}{d\tilde{t}} = -\left(\alpha + \frac{\gamma}{2}\right)r + \left(1 - \frac{\gamma}{2}\right)\alpha p - \alpha^2\beta rp + \frac{\gamma}{2}, \tag{B.11a}$$

$$\frac{dp}{d\tilde{t}} = \left(1 - \frac{\gamma}{2\alpha}\right)r - \left(1 + \frac{\gamma}{2}\right)p - \alpha\beta rp + \frac{\gamma}{2\alpha}, \tag{B.11b}$$

Appendix C. Large β asymptotic analysis

Setting $\beta = \frac{1}{\epsilon}$ and dropping the tilde, the system (5.3) (also (B.6)) becomes

$$\epsilon\frac{dr}{dt} = \epsilon\alpha(p - r) + \alpha^2(q - rp), \tag{C.1a}$$

$$\epsilon\frac{dp}{dt} = \epsilon(r - p) + \alpha(q - rp), \tag{C.1b}$$

$$\frac{dq}{dt} = \gamma(pr - q), \tag{C.1c}$$

with initial conditions

$$r(0) = 1, \qquad p(0) = 0, \qquad q(0) = 0. \tag{C.2}$$

Conservation of receptor now reads

$$1 = r + \alpha p + \frac{2\alpha^2}{\epsilon\gamma}q, \tag{C.3}$$

or

$$\epsilon = \epsilon r + \epsilon\alpha p + \frac{2\alpha^2}{\gamma}q. \tag{C.4}$$

Clearly, we require $q = O(\epsilon)$. An expression for q is given by

$$q = \frac{\gamma\epsilon}{2\alpha^2}(1 - r - \alpha p). \tag{C.5}$$

The reduced problem is

$$\epsilon\frac{dr}{dt} = -\epsilon\left(\alpha + \frac{\gamma}{2}\right)r + \epsilon\left(1 - \frac{\gamma}{2}\right)\alpha p - \alpha^2 rp + \frac{\gamma\epsilon}{2}, \tag{C.6a}$$

$$\epsilon\frac{dp}{dt} = \epsilon\left(1 - \frac{\gamma}{2\alpha}\right)r - \epsilon\left(1 + \frac{\gamma}{2}\right)p - \alpha rp + \frac{\gamma\epsilon}{2\alpha}, \tag{C.6b}$$

$$r(0) = 1, \quad p(0) = 0. \tag{C.6c}$$

where conservation gives

$$q = \frac{\gamma\epsilon}{2\alpha^2}(1 - r - \alpha p). \tag{C.6d}$$

Now we consider analysing the system (C.1) or the reduced system (C.6).

C.1. Numerical results and timescales

In Fig. C.1, we show an example numerical solution on a log–log scale. It is clear that for $t = O(\epsilon)$, the following scalings for the dependent variables in this *inner layer* (ie. on this timescale) or *initial layer* are appropriate:

$$t = \epsilon\tau, \qquad r = \tilde{r}, \qquad p = \epsilon\tilde{p}, \qquad q = \epsilon^2\tilde{q}.$$

On a longer timescale with $t = O(1)$, the following scalings are appropriate:

$$r = \bar{r}, \qquad p = \epsilon\bar{p}, \qquad q = \epsilon\bar{q}.$$

On a shifted timescale with $t = O(1)$, we see the system approaching equilibrium, and the following scalings are appropriate:

$$r = \epsilon^{\frac{1}{2}}\hat{r}, \qquad p = \epsilon^{\frac{1}{2}}\hat{p}, \qquad q = \epsilon\hat{q}.$$

C.2. Inner solution

Under the inner layer scalings

$$t = \epsilon\tau, \qquad r = \tilde{r}, \qquad p = \epsilon\tilde{p}, \qquad q = \epsilon^2\tilde{q}, \tag{C.7}$$

the governing system (C.1) gives:

$$\frac{d\tilde{r}}{d\tau} = \epsilon\alpha(\epsilon\tilde{p} - \tilde{r}) + \epsilon\alpha^2(\epsilon\tilde{q} - \tilde{r}\tilde{p}), \tag{C.8a}$$

$$\frac{d\tilde{p}}{d\tau} = \tilde{r} - \epsilon\tilde{p} + \alpha(\epsilon\tilde{q} - \tilde{r}\tilde{p}), \tag{C.8b}$$

$$\frac{d\tilde{q}}{d\tau} = \gamma(\tilde{p}\tilde{r} - \epsilon\tilde{q}), \tag{C.8c}$$

with initial conditions

$$\tilde{r}(0) = 1, \qquad \tilde{p}(0) = 0, \qquad \tilde{q}(0) = 0. \tag{C.8d}$$

Considering expansions of the form

$$\tilde{r} \approx \tilde{r}_0 + \epsilon^{\frac{1}{2}}\tilde{r}_1 + \ldots, \quad \tilde{p} \approx \tilde{p}_0 + \epsilon^{\frac{1}{2}}\tilde{p}_1 + \ldots, \quad \tilde{q} \approx \tilde{q}_0 + \epsilon^{\frac{1}{2}}\tilde{q}_1 + \ldots, \tag{C.9}$$

we find, at leading order, the following system:

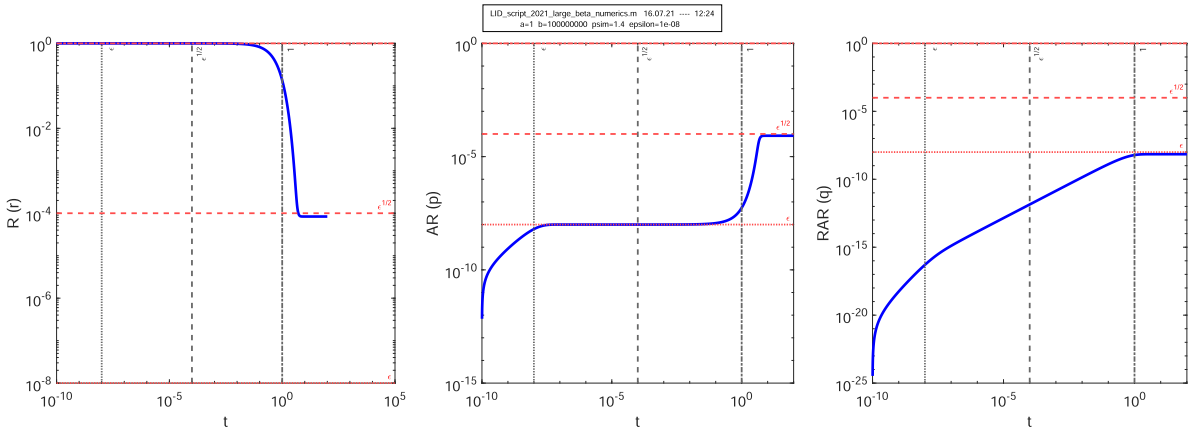

Fig. C.1. Numerical results for system (C.1), showing timescales and scalings of interest. Here, $\alpha = 1, \gamma = 1.4$ and $\epsilon = 10^{-8}$.

$$\frac{d\tilde{r}_0}{d\tau} = 0, \tag{C.10a}$$

$$\frac{d\tilde{p}_0}{d\tau} = \tilde{r}_0 - \alpha\tilde{r}_0\tilde{p}_0, \tag{C.10b}$$

$$\frac{d\tilde{q}_0}{d\tau} = \gamma\tilde{r}_0\tilde{p}_0, \tag{C.10c}$$

with initial conditions

$$\tilde{r}_0(0) = 1, \qquad \tilde{p}_0(0) = 0, \qquad \tilde{q}_0(0) = 0. \tag{C.10d}$$

This system has solution

$$\boxed{\tilde{r}_0(\tau) \equiv 1, \qquad \tilde{p}_0(\tau) = \tfrac{1-e^{-\alpha\tau}}{\alpha}, \qquad \tilde{q}_0(\tau) = \tfrac{\gamma}{\alpha^2}(\alpha\tau - 1 + e^{-\alpha\tau}).} \tag{C.11}$$

We note that $\tilde{q}_0(\tau)$ is unbounded as $\tau \to \infty$, so matching to an outer solution would not necessarily be straightforward.

Biologically, the solution $\tilde{p}_0(\tau)$ corresponds to monoexponential ligand-monomeric receptor binding kinetics. We note that $\tilde{p}_0(\tau)$ depends only on α, which controls binding kinetics but not dimerisation. This binding phase is confined to the short timescale $t = O(\epsilon)$, beyond which the effect of large dimerisation rate is seen. On this short timescale, the kinetics of q are driven by forward dimerisation only.

C.3. Intermediate solution

We seek an intermediate-time solution by considering (C.1) on the timescale $t = O(1)$ while retaining the inner species scalings for p and r, with $q = O(\epsilon)$. Specifically, we consider

$$r = \bar{r}, \qquad p = \epsilon\bar{p}, \qquad q = \epsilon\bar{q}. \tag{C.12}$$

Under these scalings, the system (C.1) becomes

$$\frac{d\bar{r}}{dt} = \alpha(\epsilon\bar{p} - \bar{r}) + \alpha^2(\bar{q} - \bar{r}\bar{p}), \tag{C.13a}$$

$$\epsilon\frac{d\bar{p}}{dt} = \bar{r} - \epsilon\bar{p} + \alpha(\bar{q} - \bar{r}\bar{p}), \tag{C.13b}$$

$$\frac{d\bar{q}}{dt} = \gamma(\bar{r}\bar{p} - \bar{q}). \tag{C.13c}$$

We find, at leading order, the following system:

$$\frac{d\bar{r}_0}{dt} = -\alpha\bar{r}_0 + \alpha^2(\bar{q}_0 - \bar{r}_0\bar{p}_0), \tag{C.14a}$$

$$0 = \bar{r}_0 - \alpha(\bar{q}_0 - \bar{r}_0\bar{p}_0), \tag{C.14b}$$

$$\frac{d\bar{q}}{dt} = \gamma(\bar{r}_0\bar{p}_0 - \bar{q}_0). \tag{C.14c}$$

The dominant reactions on this timescale are forward binding of ligand to monomeric receptor and reversible dimerisation. The system (C.14) has solutions

$$\bar{r}_0(t) = Ce^{-2\alpha t}, \qquad \bar{p}_0(t) = \frac{1}{\alpha} - \frac{\gamma}{2\alpha^2} + \frac{D}{C}e^{2\alpha t}, \qquad \bar{q}_0(t) = D - C\frac{\gamma}{2\alpha^2}e^{-2\alpha t},$$

where C and D are constants. These constants are found by matching to the inner solutions. By requiring

$$\lim_{t\to 0}\bar{r}_0(t) = \lim_{\tau\to\infty}\tilde{r}_0(\tau), \qquad \text{and} \qquad \lim_{t\to 0}\bar{p}_0(t) = \lim_{\tau\to\infty}\tilde{p}_0(\tau), \tag{C.15}$$

we find that

$$C = 1, \qquad D = \frac{\gamma}{2\alpha^2},$$

which gives the leading order solutions

$$\boxed{\bar{r}_0(t) = e^{-2\alpha t}, \qquad \bar{p}_0(t) = \tfrac{1}{\alpha} + \tfrac{\gamma}{2\alpha^2}\left(e^{2\alpha t} - 1\right), \qquad \bar{q}_0(t) = \tfrac{\gamma}{2\alpha^2}\left(1 - e^{-2\alpha t}\right).} \tag{C.16}$$

We note here that the observed decay constant of the receptor concentration, 2α, is due to both free ligand and receptor-bound ligand binding available monomeric receptors. Also, we note the exponential growth and decay terms in the solution on this timescale. The intermediate solutions will be matched to outer solutions in an "overlap" region, which approach finite nontrivial equilibrium values.

C.4. Outer solution

Under the outer solution scalings

$$r = \epsilon^{\frac{1}{2}}\hat{r}, \qquad p = \epsilon^{\frac{1}{2}}\hat{p}, \qquad q = \epsilon\hat{q}, \tag{C.17}$$

the governing system (C.1) gives:

$$\epsilon^{\frac{1}{2}}\frac{d\hat{r}}{dt} = \epsilon^{\frac{1}{2}}\alpha(\hat{p} - \hat{r}) + \alpha^2(\hat{q} - \hat{r}\hat{p}), \tag{C.18a}$$

$$\epsilon^{\frac{1}{2}}\frac{d\hat{p}}{dt} = \epsilon^{\frac{1}{2}}(\hat{r} - \hat{p}) + \alpha(\hat{q} - \hat{r}\hat{p}), \tag{C.18b}$$

$$\frac{d\hat{q}}{dt} = \gamma(\hat{p}\hat{r} - \hat{q}). \tag{C.18c}$$

Considering expansions of the form

$$\hat{r} \approx \hat{r}_0 + \epsilon^{\frac{1}{2}}\hat{r}_1 + \ldots, \quad \hat{p} \approx \hat{p}_0 + \epsilon^{\frac{1}{2}}\hat{p}_1 + \ldots, \quad \hat{q} \approx \hat{q}_0 + \epsilon^{\frac{1}{2}}\hat{q}_1 + \ldots, \tag{C.19}$$

we find, at leading order, the following system:

$$0 = \hat{q}_0 - \hat{r}_0\hat{p}_0, \tag{C.20a}$$

$$0 = \hat{q}_0 - \hat{r}_0\hat{p}_0, \tag{C.20b}$$

$$\frac{d\hat{q}_0}{dt} = 0. \tag{C.20c}$$

This system's solutions satisfy

$$\hat{q}_0(t) \equiv const, \qquad \hat{p}_0(t) = \frac{\hat{q}_0(t)}{\hat{r}_0(t)}. \tag{C.21}$$

Matching to the long-term behaviour of $\bar{q}_0(t)$ in (C.16), we find that

$$\hat{q}_0(t) \equiv \frac{\gamma}{2\alpha^2}, \qquad \hat{p}_0(t) = \frac{\gamma}{2\alpha^2\hat{r}_0(t)}. \tag{C.22}$$

To determine the dynamics of the leading order system, we consider $O\left(\epsilon^{\frac{1}{2}}\right)$ terms in the first two equations of (C.18), which give the system

$$\frac{d\hat{r}_0}{dt} = \alpha(\hat{p}_0 - \hat{r}_0) + \alpha^2(\hat{q}_1 - \hat{r}_1\hat{p}_0 - \hat{r}_0\hat{p}_1), \tag{C.23a}$$

$$\frac{d\hat{p}_0}{dt} = \hat{p}_0 - \hat{r}_0 + \alpha(\hat{q}_1 - \hat{r}_1\hat{p}_0 - \hat{r}_0\hat{p}_1). \tag{C.23b}$$

We can eliminate the nonlinear terms to give a single ODE:

$$\frac{d\hat{r}_0}{dt} - \alpha\frac{d\hat{p}_0}{dt} = 2\alpha(\hat{p}_0 - \hat{r}_0). \tag{C.24}$$

We can now make progress by using the second relationship in (C.22) to write

$$\frac{d\hat{p}_0}{dt} = -\frac{\gamma}{2\alpha^2\hat{r}_0^2}\frac{d\hat{r}_0}{dt}.$$

Substituting for both $\hat{p}_0$ and $\frac{d\hat{p}_0}{dt}$ in (C.24) gives the ODE for the outer solution $\hat{r}_0$ as

$$\frac{d\hat{r}_0}{dt} = \frac{2\hat{r}_0(\gamma - 2\alpha^2\hat{r}_0^2)}{\gamma + 2\alpha\hat{r}_0^2}. \tag{C.25}$$

We find the solution to this separable ODE to be given implicitly by

$$\log \hat{r}_0 - \frac{(\alpha+1)\log(2\alpha^2\hat{r}_0^2-\gamma)}{2\alpha} = 2t + c_1, \tag{C.26}$$

for a constant c_1. Our leading order outer solutions $\hat{r}_0, \hat{p}_0, \hat{q}_0$, may thus be summarised and computed as follows:

$$\log \hat{r}_0(t) - \frac{(\alpha+1)\log(2\alpha^2\hat{r}_0^2(t)-\gamma)}{2\alpha} = 2t + c_1, \tag{C.27a}$$

$$\hat{p}_0(t) = \frac{\gamma}{2\alpha^2\hat{r}_0(t)}, \tag{C.27b}$$

$$\hat{q}_0(t) \equiv \frac{\gamma}{2\alpha^2}. \tag{C.27c}$$

Biologically, ligand binding continues on this timescale, with reversible dimerisation in approximate equilibrium.

The single integration constant c_1 in (C.27) can be found by matching to the intermediate solution for $\bar{r}_0$ in (C.16). For that we take into account the scalings (C.12) and (C.17) which gives

$$\hat{r}_0(t) \sim \epsilon^{-\frac{1}{2}}\bar{r}_0(t), \tag{C.28}$$

in the region where these solutions should overlap. Upon substituting this into (C.27a) and writing the log-terms into one term, we find

$$\begin{aligned} &\log \frac{\epsilon^{-\frac{1}{2}}\bar{r}_0(t)}{\left(2\alpha^2\epsilon^{-1}\bar{r}_0^2(t)-\gamma\right)^{\frac{(\alpha+1)}{2\alpha}}} = 2t + c_1, \\ \Rightarrow\ &\frac{\epsilon^{-\frac{1}{2}}\bar{r}_0(t)}{\left(2\alpha^2\epsilon^{-1}\bar{r}_0^2(t)-\gamma\right)^{\frac{(\alpha+1)}{2\alpha}}} = e^{2t+c_1}, \\ \Rightarrow\ &\frac{\epsilon^{\frac{1}{2\alpha}}\bar{r}_0(t)}{\left(2\alpha^2\bar{r}_0^2(t)-\epsilon\gamma\right)^{\frac{(\alpha+1)}{2\alpha}}} = e^{2t+c_1}, \end{aligned} \tag{C.29}$$

where in the last step we multiply both the denominator and the numerator by $(\epsilon)^{\frac{(\alpha+1)}{2\alpha}}$.

Then, we find to leading order

$$\begin{aligned} &\frac{\epsilon^{\frac{1}{2\alpha}}\bar{r}_0(t)}{\left(2\alpha^2\bar{r}_0^2(t)\right)^{\frac{(\alpha+1)}{2\alpha}}} = e^{2t+c_1}, \\ \Rightarrow\ &\left(\bar{r}_0(t)\right)^{-\frac{1}{\alpha}} = \epsilon^{-\frac{1}{2\alpha}}\left(2\alpha^2\right)^{\frac{(\alpha+1)}{2\alpha}}e^{2t+c_1}, \\ \Rightarrow\ &\bar{r}_0(t) = \epsilon^{\frac{1}{2}}\left(2\alpha^2\right)^{\frac{-(\alpha+1)}{2}}e^{-2t\alpha-\alpha c_1}. \end{aligned} \tag{C.30}$$

Thus, the expression $\bar{r}_0$ is identical for that in the intermediate region in (C.16) when we choose

$$\begin{aligned} &\epsilon^{\frac{1}{2}}\left(2\alpha^2\right)^{\frac{-(\alpha+1)}{2}}e^{-\alpha c_1} = 1, \\ \Rightarrow\ &\epsilon^{\frac{1}{2}}\left(2\alpha^2\right)^{\frac{-(\alpha+1)}{2}} = e^{\alpha c_1}, \\ \Rightarrow\ &\frac{1}{\alpha}\ \log\left(\epsilon^{\frac{1}{2}}\left(2\alpha^2\right)^{\frac{-(\alpha+1)}{2}}\right) = c_1, \\ \Rightarrow\ &\frac{\log\left(\epsilon\left(2\alpha^2\right)^{-(\alpha+1)}\right)}{2\alpha} = c_1. \end{aligned} \tag{C.31}$$

In summary, we have

$$\boxed{\log \hat{r}_0(t) - \frac{(\alpha+1)\log|\gamma-2\alpha^2\hat{r}_0^2(t)|}{2\alpha} = 2t + c_1, \qquad c_1 = \frac{1}{2\alpha}\log\frac{\epsilon}{\left(2\alpha^2\right)^{\alpha+1}},} \tag{C.32}$$

$$\boxed{\hat{p}_0(t) = \frac{\gamma}{2\alpha^2\hat{r}_0(t)}, \qquad \hat{q}_0(t) \equiv \frac{\gamma}{2\alpha^2}.} \tag{C.33}$$

Appendix D. Large γ asymptotics

Setting $\gamma = \frac{1}{\epsilon}$ and dropping the tilde, the system (5.3) becomes

$$\frac{dr}{dt} = \alpha(p-r) + \alpha^2\beta(q-rp), \tag{D.1a}$$

$$\frac{dp}{dt} = r - p + \alpha\beta(q-rp), \tag{D.1b}$$

$$\epsilon\frac{dq}{dt} = pr - q, \tag{D.1c}$$

with initial conditions

$$r(0) = 1, \qquad p(0) = 0, \qquad q(0) = 0. \tag{D.2}$$

Conservation of receptor now reads

$$1 = r + \alpha p + 2\alpha^2\beta\epsilon q. \tag{D.3}$$

The reduced problem is

$$\epsilon\frac{dr}{dt} = -\left(\epsilon\alpha + \frac{1}{2}\right)r + \alpha\left(\epsilon - \frac{1}{2}\right)p - \epsilon\alpha^2\beta rp + \frac{1}{2\alpha}, \tag{D.4a}$$

$$\epsilon\frac{dp}{dt} = \left(\epsilon - \frac{1}{2\alpha}\right)r - \left(\epsilon + \frac{1}{2}\right)p - \epsilon\alpha\beta rp + \frac{1}{2\alpha}, \tag{D.4b}$$

$$r(0) = 1, \quad p(0) = 0. \tag{D.4c}$$

where conservation gives

$$q = \frac{1 - r - \alpha p}{2\alpha^2\beta\epsilon}. \tag{D.4d}$$

Now we consider analysing the system (D.1) or the reduced system (D.4).

D.1. Numerical results and timescales

In Fig. D.1, we show an example numerical solution on a log–log scale. It is clear that for $t = O(\epsilon)$, the following scalings for the dependent variables in this *inner layer* (ie. on this timescale) or *initial layer* are appropriate:

$$t = \epsilon\tau, \qquad r = \tilde{r}, \qquad p = \epsilon\tilde{p}, \qquad q = \epsilon\tilde{q}.$$

On a longer timescale with $t = O(1)$, the following scalings are appropriate:

$$r = \bar{r}, \qquad p = \bar{p}, \qquad q = \bar{q}.$$

D.2. Inner solution

Under the inner layer scalings

$$t = \epsilon\tau, \qquad r = \tilde{r}, \qquad p = \epsilon\tilde{p}, \qquad q = \epsilon\tilde{q}, \tag{D.5}$$

the governing system (D.1) gives:

$$\frac{d\tilde{r}}{d\tau} = \alpha(\epsilon^2\tilde{p} - \epsilon\tilde{r}) + \epsilon^2\alpha^2\beta(\tilde{q} - \tilde{r}\tilde{p}), \tag{D.6a}$$

$$\frac{d\tilde{p}}{d\tau} = \tilde{r} - \epsilon\tilde{p} + \epsilon\alpha\beta(\tilde{q} - \tilde{r}\tilde{p}), \tag{D.6b}$$

$$\frac{d\tilde{q}}{d\tau} = \tilde{p}\tilde{r} - \tilde{q}, \tag{D.6c}$$

with initial conditions

$$\tilde{r}(0) = 1, \qquad \tilde{p}(0) = 0, \qquad \tilde{q}(0) = 0. \tag{D.6d}$$

Considering expansions of the form

$$\begin{aligned} \tilde{r} &\approx \tilde{r}_0 + \epsilon^{\frac{1}{2}}\tilde{r}_1 + \ldots, \quad \tilde{p} \approx \tilde{p}_0 + \epsilon^{\frac{1}{2}}\tilde{p}_1 + \ldots, \quad \tilde{q} \\ &\approx \tilde{q}_0 + \epsilon^{\frac{1}{2}}\tilde{q}_1 + \ldots, \end{aligned} \tag{D.7}$$

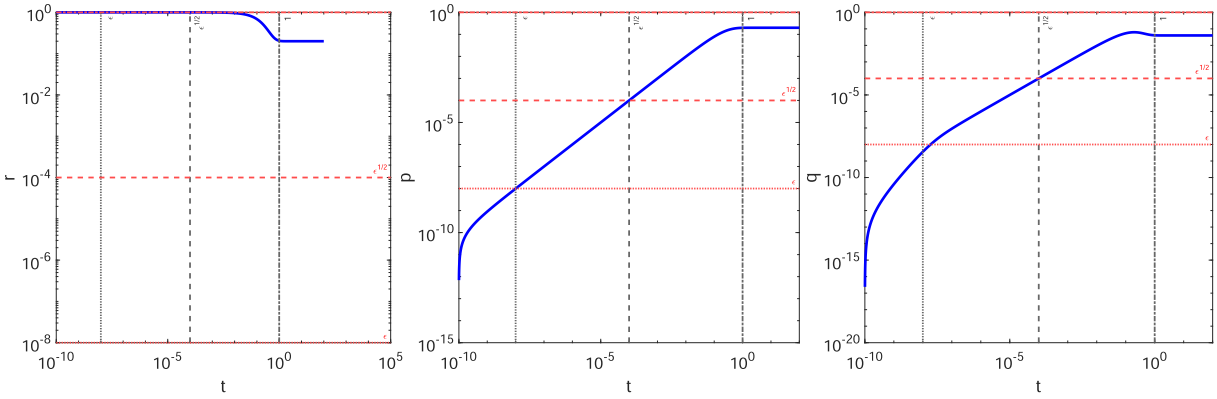

Fig. D.1. Numerical results for system (C.1), showing timescales and scalings of interest. Here, $\alpha = 4, \beta = 0.2$ and $\epsilon = 10^{-8}$.

we find, at leading order, the following system:

$$\frac{d\tilde{r}_0}{d\tau} = 0, \tag{D.8a}$$

$$\frac{d\tilde{p}_0}{d\tau} = \tilde{r}_0, \tag{D.8b}$$

$$\frac{d\tilde{q}_0}{d\tau} = \tilde{r}_0\tilde{p}_0 - \tilde{q}_0, \tag{D.8c}$$

with initial conditions

$$\tilde{r}_0(0) = 1, \qquad \tilde{p}_0(0) = 0, \qquad \tilde{q}_0(0) = 0. \tag{D.8d}$$

This system has solution

$$\boxed{\tilde{r}_0(\tau) \equiv 1, \qquad \tilde{p}_0(\tau) = \tau, \qquad \tilde{q}_0(\tau) = e^{-\tau} + \tau - 1.} \tag{D.9}$$

Both $\tilde{p}_0(\tau)$ and $\tilde{q}_0(\tau)$ is unbounded as $\tau \to \infty$, so matching to an outer solution would not necessarily be straightforward.

Biologically, the dominant reactions on this timescale are the forward binding of ligand to monomeric receptor, which only affects *AR* dynamics, and the reversible dimerisation.

D.3. Outer solution

For the outer solution

$$r = \hat{r}, \qquad p = \hat{p}, \qquad q = \hat{q}, \tag{D.10}$$

to the governing system (D.1), we considering expansions of the form

$$\hat{r} \approx \hat{r}_0 + \epsilon^{\frac{1}{2}}\hat{r}_1 + \ldots, \quad \hat{p} \approx \hat{p}_0 + \epsilon^{\frac{1}{2}}\hat{p}_1 + \ldots, \quad \hat{q} \approx \hat{q}_0 + \epsilon^{\frac{1}{2}}\hat{q}_1 + \ldots. \tag{D.11}$$

We find, at leading order, the following system:

$$\frac{d\hat{r}_0}{dt} = \alpha(\hat{p}_0 - \hat{r}_0), \tag{D.12a}$$

$$\frac{d\hat{p}_0}{dt} = \hat{p}_0 - \hat{r}_0, \tag{D.12b}$$

$$0 = \hat{r}_0\hat{p}_0 - \hat{q}_0. \tag{D.12c}$$

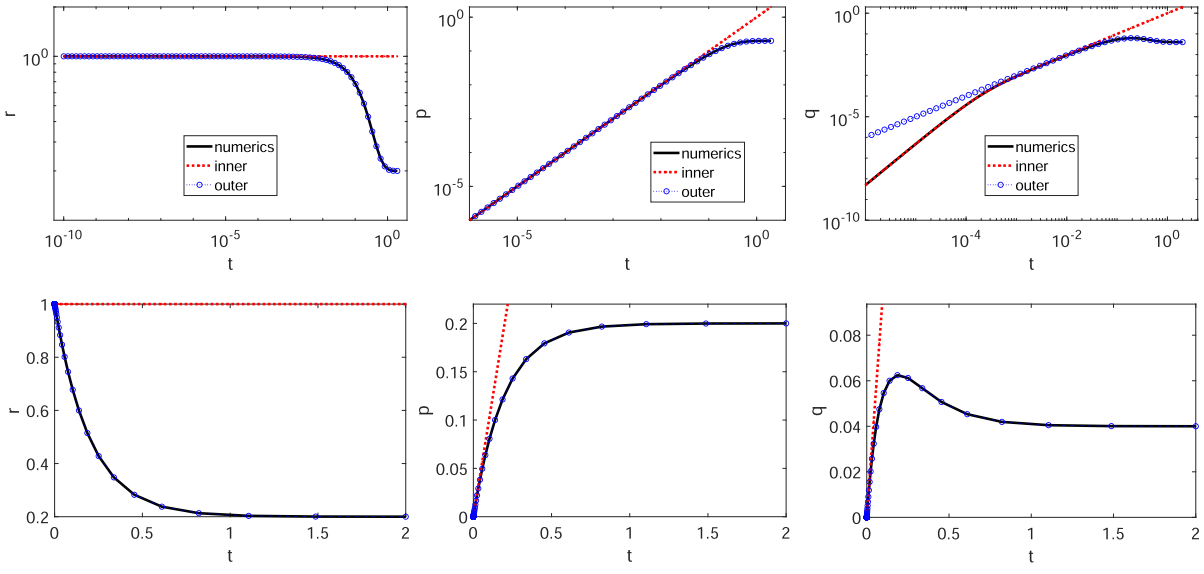

Fig. D.2. Numerical and asymptotic results for system (D.1), showing timescales and scalings of interest. Here, $\alpha = 4, \beta = 0.2$ and $\epsilon = 10^{-4}$.

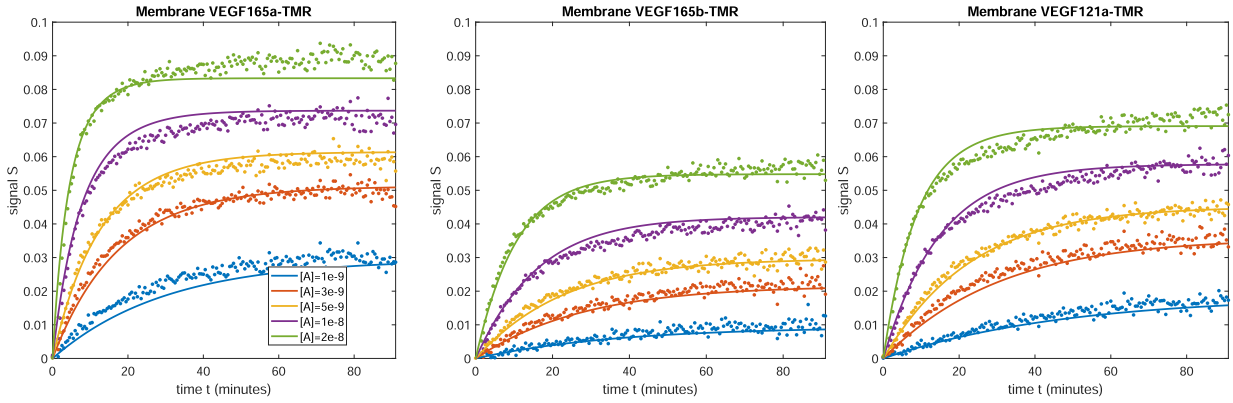

Fig. E.1. Data published in Peach et al. (2019) are used to estimate the model parameters. Experiments were performed using five concentrations of three different VEGF isoforms (VEGF $_{165}$a-TMR, VEGF $_{165}$b-TMR and VEGF $_{121}$a-TMR) and the signal $S(t)$ (2.3) is recorded. Parameters a and R_{tot} are constrained to be equal across all experiments. Parameter values returned can be seen in Table E.1.

Table E.1
Estimated parameters returned from fitting to the data, as seen in Fig. 6.1. Units: k_+ (M^{-1} min^{-1}), k_- (min^{-1}), R_{tot} (M).

	a	k_+	k_-	ψ_+	ψ_-	R_{tot}
$VEGF_{165}$a-TMR	2.78×10^7	6.85×10^6	3.44×10^{-2}	1.95×10^3	1.79×10^3	3.59×10^{-9}
$VEGF_{165}$b-TMR	2.78×10^7	1.48×10^6	8.04×10^{-2}	6.30×10^3	1.65×10^2	3.59×10^{-9}
$VEGF_{121}$a-TMR	2.78×10^7	2.23×10^6	5.09×10^{-2}	2.61×10^4	1.63×10^3	3.59×10^{-9}

This system's solutions satisfy

$$\hat{r}_0(t) = B + A\alpha e^{-(\alpha+1)t}, \qquad \hat{p}_0(t) = B - Ae^{-(\alpha+1)t},$$
$$\hat{q}_0(t) = B^2 + AB(\alpha-1)e^{-(\alpha+1)t} - A^2 e^{-2(\alpha+1)t}, \tag{D.14}$$

for constants A and B to be found by matching to the inner solutions. By requiring that

$$\lim_{\tau\to\infty} \tilde{r}_0(\tau) = \lim_{t\to 0} \hat{r}_0(t),$$

we find that

$$B = 1 - A\alpha.$$

Also, we require that

$$\tilde{p}_0(\tau) \sim \hat{p}_0(t) \qquad \text{for} \quad t = \epsilon^\delta,\ \tau = \epsilon^{-\delta},$$

for $0 < \delta < 1$. Taking, for example, $\delta = \frac{1}{2}$, we find that

$$A = B = \frac{1}{\alpha+1}.$$

Then the outer solution is given by

$$\hat{r}_0(t) = \frac{1+\alpha e^{-(\alpha+1)t}}{1+\alpha}, \qquad \hat{p}_0(t) = \frac{1-e^{-(\alpha+1)t}}{1+\alpha},$$
$$\hat{q}_0(t) = \frac{1+(\alpha-1)e^{-(\alpha+1)t} - \alpha e^{-2(\alpha+1)t}}{(1+\alpha)^2}. \tag{D.15}$$

Biologically, the dominant reactions on this timescale are the reversible binding of ligand to monomeric receptor, while reversible dimerisation has approximately reached equilibrium due to the rapid undimerisation.

In Fig. D.2, we show example numerical results and asymptotic approximations. Agreement between the numerical solution and the inner and outer approximations is clear for the inner and outer timescales.

Appendix E. Data fitting

In Fig. E.1 and Table E.1, we show illustrative results of an alternative parameter estimation implementation, with a and R_{tot} fixed across all parameter sets, as described in Section 6. We note the order-of-magnitude agreement with the results shown in Fig. 6.1 and Table 6.1, where a and R_{tot} were estimated independently for each of the three experiments.

References

Alarcón, T., Page, K.M., 2007. Mathematical models of the VEGF receptor and its role in cancer therapy. J. Royal Soc. Interface 4 (13), 283–304.
Bridge, L., 2009. Modeling and simulation of inverse agonism dynamics. Methods Enzymol. 485, 559–582.
Bridge, L., King, J., Hill, S., Owen, M., 2010. Mathematical modelling of signalling in a two-ligand g-protein coupled receptor system: Agonist–antagonist competition. Math. Biosci. 223 (2), 115–132.
Chis, O., Banga, J.R., Balsa-Canto, E., 2011. Methods for checking structural identifiability of nonlinear biosystems: A critical comparison. IFAC Proceedings Volumes 44 (1), 10585–10590.
Franco, R., Casadó, V., Mallol, J., Ferré, S., Fuxe, K., Cortés, A., Ciruela, F., Lluis, C., Canela, E.I., 2005. Dimer-based model for heptaspanning membrane receptors. Trends Biochemical Sci. 30 (7), 360–366.
Franco, R., Casadó, V., Mallol, J., Ferrada, C., Ferré, S., Fuxe, K., Cortés, A., Ciruela, F., Lluis, C., Canela, E.I., 2006. The two-state dimer receptor model: a general model for receptor dimers. Mol. Pharmacol. 69 (6), 1905–1912.
Godfrey, K., DiStefano III, J., 1985. Identifiability of model parameter. IFAC Proceedings Volumes 18 (5), 89–114.
Gopalakrishnan, M., Forsten-Williams, K., Täuber, U.C., 2004. Ligand-induced coupling versus receptor pre-association: cellular automaton simulations of FGF-2 binding. J. Theor. Biol. 227 (2), 239–251.
Grewal, M., Glover, K., 1976. Identifiability of linear and nonlinear dynamical systems. IEEE Trans. Automatic Control 21 (6), 833–837.
Hoops, S., Sahle, S., Gauges, R., Lee, C., Pahle, J., Simus, N., Singhal, M., Xu, L., Mendes, P., Kummer, U., 2006. Copasi—a complex pathway simulator. Bioinformatics 22 (24), 3067–3074.
Janzén, D.L., Bergenholm, L., Jirstrand, M., Parkinson, J., Yates, J., Evans, N.D., Chappell, M.J., 2016. Parameter identifiability of fundamental pharmacodynamic models. Front. Physiol. 7, 590.
Kenakin, T., 2009. A pharmacology primer: theory, application and methods. Academic Press.

Kilpatrick, L.E., Friedman-Ohana, R., Alcobia, D.C., Riching, K., Peach, C.J., Wheal, A.J., Briddon, S.J., Robers, M.B., Zimmerman, K., Machleidt, T., et al., 2017. Real-time analysis of the binding of fluorescent VEGF165a to VEGFR2 in living cells: effect of receptor tyrosine kinase inhibitors and fate of internalized agonist-receptor complexes. Biochem. Pharmacol. 136, 62–75.

Klein, P., Mattoon, D., Lemmon, M.A., Schlessinger, J., 2004. A structure-based model for ligand binding and dimerization of EGF receptors. Proc. Nat. Acad. Sci. 101 (4), 929–934.

Lauffenburger, D.A., Linderman, J., 1993. Receptors: models for binding, trafficking, and signaling. Oxford University Press.

Mac Gabhann, F., Popel, A.S., 2004. Model of competitive binding of vascular endothelial growth factor and placental growth factor to VEGF receptors on endothelial cells. Am. J. Physiol.-Heart Circulatory Physiol. 286 (1), H153–H164.

Mac Gabhann, F., Popel, A.S., 2007. Dimerization of vegf receptors and implications for signal transduction: a computational study. Biophys. Chem. 128 (2), 125–139.

Mac Gabhann, F., Qutub, A.A., Annex, B.H., Popel, A.S., 2010. Systems biology of pro-angiogenic therapies targeting the VEGF system. Wiley Interdisciplinary Reviews: Systems Biology and Medicine 2 (6), 694–707.

Maruyama, I., 2014. Mechanisms of activation of receptor tyrosine kinases: monomers or dimers. Cells 3 (2), 304–330.

Matlab, the MathWorks Inc.

Mayawala, K., Vlachos, D.G., Edwards, J.S., 2006. Spatial modeling of dimerization reaction dynamics in the plasma membrane: Monte carlo vs. continuum differential equations. Biophys. Chem. 121 (3), 194–208.

May, L.T., Bridge, L.J., Stoddart, L.A., Briddon, S.J., Hill, S.J., 2011. Allosteric interactions across native adenosine-a3 receptor homodimers: quantification using single-cell ligand-binding kinetics. FASEB J. 25 (10), 3465–3476.

Milligan, G., 2004. G protein-coupled receptor dimerization: function and ligand pharmacology. Mol. Pharmacol. 66 (1), 1–7.

Milligan, G., 2006. G-protein-coupled receptor heterodimers: pharmacology, function and relevance to drug discovery. Drug Discovery Today 11 (11), 541–549.

Milligan, G., 2013. The prevalence, maintenance, and relevance of g protein–coupled receptor oligomerization. Mol. Pharmacol. 84 (1), 158–169.

Murray, J.D., 2007. Mathematical biology: I. An introduction, Vol. 17. Springer Science & Business Media.

Olsson, A.-K., Dimberg, A., Kreuger, J., Claesson-Welsh, L., 2006. VEGF receptor signalling – in control of vascular function. Nature Rev. Mol. Cell Biol. 7 (5), 359.

Personal communication between Lloyd Bridge and C. J. Peach, Excel data files for time courses published in [Peach 2019] provided for data fitting purposes, courtesy of C. J. Peach and the Institute of cell signalling, University of Nottingham.

Peach, C.J., Mignone, V.W., Arruda, M.A., Alcobia, D.C., Hill, S.J., Kilpatrick, L.E., Woolard, J., 2018. Molecular pharmacology of VEGF-A isoforms: binding and signalling at VEGFR2. Int. J. Mol. Sci. 19 (4), 1264.

Peach, C.J., Kilpatrick, L.E., Woolard, J., Hill, S.J., 2019. Comparison of the ligand-binding properties of fluorescent VEGF-a isoforms to VEGF receptor 2 in living cells and membrane preparations using nanobret. British J. Pharmacol. 176 (17), 3220–3235.

Peletier, L.A., Gabrielsson, J., 2018. Impact of mathematical pharmacology on practice and theory: four case studies. J. Pharmacokinetics Pharmacodynamics 45 (1), 3–21.

Pohjanpalo, H., 1978. System identifiability based on the power series expansion of the solution. Math. Biosci. 41 (1–2), 21–33.

Shibuya, M., 2011. Vascular endothelial growth factor (VEGF) and its receptor (VEGFR) signaling in angiogenesis: a crucial target for anti-and pro-angiogenic therapies. Genes Cancer 2 (12), 1097–1105.

Stuttfeld, E., Ballmer-Hofer, K., 2009. Structure and function of VEGF receptors. IUBMB life 61 (9), 915–922.

van der Graaf, P.H., Benson, N., Peletier, L.A., 2016. Topics in mathematical pharmacology. J. Dyn. Diff. Eqs. 28 (3–4), 1337–1356.

Vera, J., Millat, T., Kolch, W., Wolkenhauer, O., 2008. Dynamics of receptor and protein transducer homodimerisation. BMC Syst. Biol. 2 (1), 92.

Wanant, S., Quon, M.J., 2000. Insulin receptor binding kinetics: modeling and simulation studies. J. Theor. Biol. 205 (3), 355–364.

White, C., Bridge, L.J., 2019. Ligand binding dynamics for pre-dimerised g protein-coupled receptor homodimers: linear models and analytical solutions. Bull. Math. Biol. 81 (9), 3542–3574.

Wofsy, C., Goldstein, B., Lund, K., Wiley, H., 1992. Implications of epidermal growth factor (EGF) induced egf receptor aggregation. Biophys. J. 63 (1), 98–110.

Woodroffe, P., Bridge, L., King, J., Hill, S., 2009. Modelling the activation of g-protein coupled receptors by a single drug. Mathe. Biosci. 219 (1), 32–55.

Woodroffe, P., Bridge, L., King, J., Chen, C., Hill, S., 2010. Modelling of the activation of g-protein coupled receptors: drug free constitutive receptor activity. J. Math. Biol. 60 (3), 313–346.

Zhou, B., Giraldo, J., 2018. An operational model for GPCR homodimers and its application in the analysis of biased signaling. Drug Discovery Today 23 (9), 1591–1595.